

# Mobility-enhanced MPC for Legged Locomotion on Rough Terrain

Niraj Rathod<sup>1,2</sup>, Angelo Bratta<sup>2</sup>, Michele Focchi<sup>2</sup>, Mario Zanon<sup>1</sup>, Octavio Villarreal<sup>2</sup>, Claudio Semini<sup>2</sup> and Alberto Bemporad<sup>1</sup>

**Abstract**—Re-planning in legged locomotion is crucial to track a given set-point while adapting to the terrain and rejecting external disturbances. In this work, we propose a real-time Nonlinear Model Predictive Control (NMPC) tailored to a legged robot for achieving dynamic locomotion on a wide variety of terrains. We introduce a mobility-based criterion to define an NMPC cost that enhances the locomotion of quadruped robots while maximizing leg mobility and staying far from kinematic limits. Our NMPC is based on the real-time iteration scheme that allows us to re-plan online at 25 Hz with a time horizon of 2 seconds. We use the single rigid body dynamic model defined in the center of mass frame that allows to increase the computational efficiency. In simulations, the NMPC is tested to traverse a set of pallets of different sizes, to walk into a V-shaped chimney, and to locomote over rough terrain. We demonstrate the effectiveness of our NMPC with the mobility feature that allowed IIT’s 87.4 kg quadruped robot HyQ to achieve an omni-directional walk on flat terrain, to traverse a static pallet, and to adapt to a repositioned pallet during a walk in real experiments.

**Index Terms**—Mobility, Nonlinear Model Predictive Control, Online planning, Legged locomotion

## I. INTRODUCTION

The main advantage of legged robots with respect to their wheeled counterpart is their ability to traverse unstructured environment such as stairs, obstacles, and debris. However, the control of legged robots poses complex problems related to underactuation (the body is controlled only indirectly through the legs), and to the hybrid nature of the forces required to generate motion, since the robot needs to establish and interrupt contact between its feet and the ground. The control design for legged robots was initially dealt with by using heuristic approaches which yielded remarkable results such as in the walking machines from Raibert [1], the virtual model control of Pratt et al. [2] and in the heuristic locomotion planning for quadrupedal robots by Focchi et al. [3]. However, heuristic approaches have several limitations, for example: 1) they cannot be easily generalized to all kinds of terrain and motion; 2) they cannot account for the future state of the robot hence, they have no possibility to guarantee physical feasibility of the planned trajectories. The challenge of avoiding these undesirable *myopic* behaviors in heuristic planning approaches has motivated the research towards new optimization-based predictive locomotion planning.

<sup>1</sup> The authors are with the IMT School for Advanced Studies Lucca, Lucca, Italy. name.surname@imtlucca.it

<sup>2</sup> The authors are with the Dynamic Legged Systems Lab, Istituto Italiano di Tecnologia (IIT), Genova, Italy. name.surname@iit.it



Fig. 1: IIT’s quadruped robot HyQ traversing a pallet with the mobility enhanced real-time NMPC.

Formulating the locomotion planning problem as an optimization problem allows one to represent high-level locomotion tasks and system dynamics using cost functions and constraints, respectively. Besides robot dynamics, the locomotion tasks should also respect the contact dynamics such as unilateral force and friction cone constraints, that are critical to stabilize the locomotion. The use of optimization techniques to design Whole-Body Control (WBC) has enabled legged robots to overcome challenging terrains [4], to traverse soft terrains [5] and to be versatile in terms of type of gait and motions that a legged robot can achieve [6]. The aforementioned examples are based on the solution of a Quadratic Program that only considers the instantaneous [7] effects of the joint torques on the robot’s base. Further, similar to heuristic approaches mentioned earlier, these approaches do not consider the information about the future states of the robot and hence cannot assure recursive feasibility.

In order to address this issue, several approaches studied Trajectory Optimization (TO) based locomotion planning considering the full dynamics of the robot [8, 9]. However, these approaches often suffer from high computational time hence they are restricted to *offline* use. In general, offline (open loop) planners [10, 11] neither adapt to quick terrain changes nor cope with state drifts and uncertainties. To address this issue the concept of *online* re-planning can be used. Online re-planning can intrinsically cope with the problem of error accumulation in planned motion that is common in

real scenarios. For online re-planning, MPC has gained broad interest in the robotics community for legged locomotion. Moreover, the intrinsic feedback mechanism offered by MPC can compensate for modeling errors and disturbances acting on the system provided that the MPC is executed at a sufficiently high rate in closed-loop. An MPC formulation with a careful choice of the dynamic model is typically required to achieve a desired re-planning frequency in closed-loop, given the limited computational resources available for online computations. For example, using a full dynamics model of legged robots inside MPC [12, 13] with long prediction horizon results in an optimization problem which requires excessive computations for real-time deployment at high sampling rates. Using approximate models is a way to reduce the complexity of the optimization, trading the accuracy with computational efficiency. Following this line, [14] used a Centroidal Dynamics (CD) plus a full-kinematic model to enforce the kinematic limits in TO to plan complex behaviors on the humanoid robot Atlas. The CD model considers contact forces as input and links the linear and angular momentum of the robot to the external wrench [15].

A simplified version of the CD model is the Single Rigid Body Dynamics (SRBD) model where the inertia of the legs is neglected (this model assumes massless legs) and the robot's body and legs are lumped into a single rigid body. This model is well suited for quadrupeds, since they usually concentrate their mass and inertia in the robot base, unlike humanoids. The SRBD model was used for TO [16] and MPC [17] to jointly optimize for footholds, Center of Mass (CoM) trajectories and contact forces. By further linearizing the angular part of the dynamics of the SRBD, [18] was able to achieve a variety of quadrupedal gaits in experiments but their approach was not suitable for motions that involve large variations from the horizontal orientation. The simplest among all the approximate models mentioned earlier is the Linear Inverted Pendulum Model (LIPM) and it has been used inside MPC for quadruped [19] and biped [20] locomotion. However, there are two main limitations in LIPM, namely it neglects angular dynamics and assumes constant robot height. Additionally, it does not account for friction cones, so that contact stability on non-flat terrain can not be guaranteed.

While models play an important role in obtaining computationally light MPC formulations, the choice of solution method is also paramount to achieve fast online re-planning with MPC. A Differential Dynamic Programming (DDP) based approach demonstrated the real-time performance with whole-body MPC [13] on HRP-2 humanoid. Recently, [21] proposed a DDP-based MPC using a kinodynamic model which re-plans at a low frequency of 15 Hz with a time horizon of 1 s on a quadruped. The main drawbacks of DDP based approaches are: 1) the need of writing custom-made solvers, 2) some difficulty in implementing hard-inequality and switching constraints. Hard-inequality constraints need to be implemented as penalties (e.g., with relaxed-barriers) [22] while the switching constraints are formulated using Augmented Lagrangian methods [23, 24]. Though not obvious at first sight, these methods are essentially equivalent to direct optimal control based on multiple-shooting [25] in combination with some

form of Nonlinear Programming (NLP) solvers using barrier functions in the real-time iteration scheme [26]. One such framework is provided by `acados` [27].

In addition to DDP-based MPC, there also exist a few implementations of NLP-based MPC for legged robots. One such NMPC implementation with CoM dynamics plus full kinematic model was demonstrated in [28] using a Sequential Linear Quadratic (SLQ) algorithm for a trotting gait on flat terrain. Neunert et al. [12] achieved a fast re-planning frequency of 80-170 Hz for a small time horizon of 0.5 s with their NMPC using the full dynamics of the robot, and optimizing foot locations, swing timing, and locomotion sequences along with full body dynamics. However, in the real experiments they have only demonstrated the locomotion of quadrupeds in place and slow trotting on flat terrain. Moreover, since their approach does not consider the map of the terrain, it has limited application on uneven terrain conditions. An interesting observation is that they did not see a noticeable degradation in the closed-loop performance of the NMPC when the re-planning frequency was dropped until 30 Hz, demonstrating that the predictive nature of the MPC empowers the robot to tolerate much lower re-planning frequency. A similar observation has been made in [29] with an MPC scheme which optimizes foot locations, but requires a heuristic conditioning of the cost function. In the experiments, the robot is stable if the re-planning occurs at 20 Hz, unstable for lower frequencies and the performance improvement is observed over 40 Hz.

The aforementioned approaches have been successful in controlling legged robots, but neglected an important aspect of these robots, which is usually referred to as *mobility*. In this paper, we define the mobility as the attitude of the robot leg to arbitrarily change its foot position. To achieve kinematically suitable configurations for the legs, a common heuristic is to align the robot base with the terrain inclination (estimated in [3] via fitting an averaging plane through the stance feet). This approach aims to bring the legs as close as possible to the middle of their workspaces in order to avoid the violation of the kinematic limits. Optimization of mobility allows to achieve a similar behaviour in an automatic way. Fankhauser et al. in [30] maximized mobility by encoding it in a cost function that penalizes the distance with respect to a default foot position. Recently, Cebe et al. [31] implemented TO using an SRBD model and also incorporating the feet positions in the optimization. They re-plan only at the feet touchdowns due to the high computation demand of their TO algorithm and showed experimental results on uneven terrain. Since their planner does not plan during the swing phase of the legs, they do not run their planner in an MPC fashion. Apart from the previously mentioned work, to the best of our knowledge no contribution has been made to address the mobility with MPC in legged locomotion.

#### A. Proposed Approach and Contribution

In this work, we introduce a real-time NMPC planner for rough terrain locomotion that accounts for leg mobility to drive the base orientation of our Hydraulically actuated

Quadruped (HyQ) robot [32] in real experiments. In our implementation, we employ a simplified SRBD model that describes the angular and translational dynamics of the robot base but neglects the dynamics of legs. The contributions of our work are as follows:

- We formulate an SRBD model enforcing contact sequences in an optimization-friendly way through model parameters that are updated online, rather than through complementarity constraints. This results in an NMPC formulation of lower complexity compared to alternative model formulations. We introduce a cost term which accounts for *mobility* by penalizing hip-to-foot positions that do not provide the highest mobility. This allows our NMPC to devise a robot base orientation and height that ensures high leg mobility during locomotion on rough terrain. To date, this is the first time mobility has been addressed with MPC to the best of our knowledge. We also introduce improvement features regarding *force regularization* for locomotion stability and *kinematic robustness* to account for estimation errors on the contact normals inside our NMPC that are essential for locomotion on rough terrain.
- Running an NMPC online with a long prediction horizon poses the challenge of either a high computation time or to accept a suboptimal solution. We have addressed this problem through the real-time iteration (RTI) scheme [26, 33, 34] that allowed us to run our NMPC online with a time horizon of 2s as opposed to the 0.5s used by [12]. Differently from [31] (that re-plans at each foot touchdown event), we continuously re-plan at the rate of 25 Hz. We run our NMPC on a single computer along with the rest of our locomotion framework<sup>1</sup> unlike in [31, 12] where they use dedicated computers for their TO and NMPC, respectively.
- Simulations and Experiments: We show in simulation the robot traversing a set of pallets of different dimensions placed relatively at varying distances, walking into a V-shaped chimney and lastly over a randomly generated rough terrain. We present *Experimental* results that demonstrate the capability of our NMPC to generate an omni-directional walk and to traverse a pallet for our quadruped robot HyQ, by exploiting an online evaluation of the map of the terrain and on-board state estimation. We test the re-planning capability of our approach by pushing a pallet in front of the robot while walking, such that the perception algorithms have to estimate the new pallet position and the control algorithm has to re-plan online in order to adapt to a dynamically changing environment.

The optimization is carried out with minimal heuristics from the user i.e., no reference trajectory for the robot’s height, its base roll and pitch orientation is required. The generation of the reference trajectory for the NMPC takes into account premature and delayed touchdown of the feet as well as continuously adjusting the footholds according to the robot body motion and the terrain features.

<sup>1</sup>Except the perception related modules that run on a dedicated computer

## B. Outline

The paper is organized as follows: Section II gives an of our planning pipeline whereas Section III describes the NMPC setup. The contributions about leg mobility and robustness are discussed in Section IV whereas the generation of the references and the WBC are detailed in Sections V and VI, respectively. We then summarize the RTI scheme for our NMPC in Section VII. Further, Section VIII illustrates simulation and experimental results with the HyQ robot. Finally, we draw the conclusions in Section IX.

## II. LOCOMOTION FRAMEWORK

In Fig. 2, we illustrate the planning pipeline of our locomotion framework. The *reference generator*, as discussed in Section V, takes the user input (longitudinal, lateral and angular velocity), the gait (e.g., a crawl), the initial state of the robot, and a map of the terrain to generate reference trajectories for the state  $\mathbf{x}^{\text{ref}}$  and control input  $\mathbf{u}^{\text{ref}}$  required by the NMPC. The reference generator also provides a vector of parameters  $\mathbf{a}$  to the NMPC, that includes foot locations and contact sequences. The NMPC running at 25 Hz, delivers the optimal trajectories of the state  $\mathbf{x}^{\text{p}}$  and control input  $\mathbf{u}^{\text{p}}$ , as detailed in Section III. All the components of the Whole-Body controller (highlighted with dashed box in Fig. 2) are discussed in Section VI. The *WBC interface* interpolates the optimal state  $\mathbf{x}^{\text{p}}$  at a rate of 250 Hz to generate a desired signal  $\mathbf{x}^{\text{d}}$  for a Cartesian virtual impedance controller [4]. The WBC interface also computes the feedforward wrench  $\mathbf{W}_{\text{ff}}^{\text{d}}$  that is added to a feedback wrench  $\mathbf{W}_{\text{fb}}^{\text{d}}$  that renders the Cartesian impedance. Moreover, the WBC interface provides the joint position  $\mathbf{q}_{\text{d}}$  and velocities  $\dot{\mathbf{q}}_{\text{d}}$  to a Joint Space PD controller running at 1 kHz. After acquiring the feedback and feed-forward wrenches, a Quadratic Programming (QP) optimization computes the vector of desired Ground Reaction Forces (GRFs)  $\mathbf{f}^{\text{d}}$  accounting for the friction cone constraints and penalizing the the difference between  $\mathbf{f}^{\text{d}}$  and  $\mathbf{u}^{\text{p}}$  coming from the NMPC solution. Then,  $\mathbf{f}^{\text{d}}$  is mapped to the torque vector  $\boldsymbol{\tau}^*$  that is added to the Joint Space PD torques  $\boldsymbol{\tau}_{\text{fb}}$  resulting into the total desired torque  $\boldsymbol{\tau}_{\text{d}}$ . The value  $\boldsymbol{\tau}_{\text{d}}$  is passed to a low-level joint torque controller as reference [35]. An online state estimator [36] that runs at 500 Hz provides the estimation of the robot state to all the components inside our locomotion framework that require it. A dedicated on-board computer takes inputs from an RGB-D camera (RealSense) mounted in front of the robot and generates a 2.5D heightmap at the rate of 30 Hz using the *Grid Map* library from [37]. This heightmap is later sent to the reference generator.

## III. NMPC

In our planning algorithm, we choose a real-time NMPC formulation because it has the ability to handle both the nonlinear system dynamics and the constraints, explicitly. NMPC is based on solving an Optimal Control Problem (OCP) given the current state  $\hat{\mathbf{x}}_0$  of the system. Only the first element of the optimized input trajectory is applied to the system, then the state is measured and the OCP is solved again based on the new state measurement to close the loop.

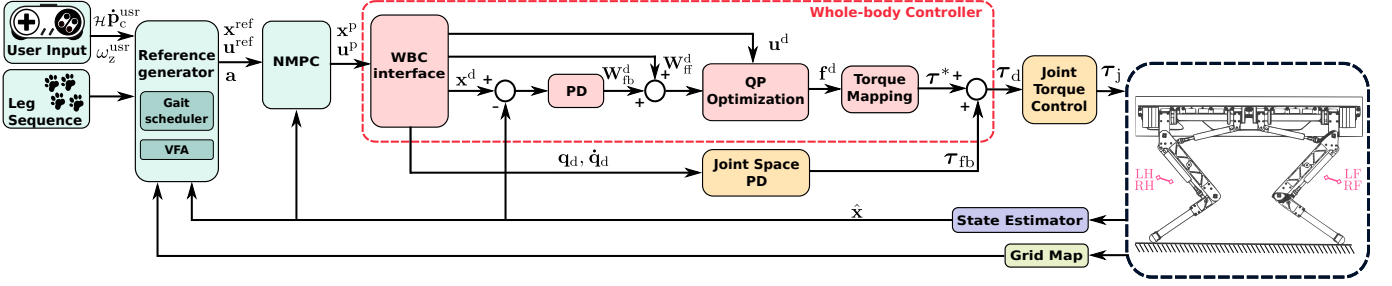


Fig. 2: Block diagram of the planning pipeline with the NMPC in our locomotion framework.

We define the decision variables as the predicted state and control input with  $\mathbf{x}^p = \{\mathbf{x}_0, \dots, \mathbf{x}_N\}$  and  $\mathbf{u}^p = \{\mathbf{u}_0, \dots, \mathbf{u}_{N-1}\}$ , respectively, such that an NLP formulation can be stated as:

$$\min_{\mathbf{x}^p, \mathbf{u}^p} \sum_{k=0}^{N-1} \ell(\mathbf{x}_k, \mathbf{u}_k, \mathbf{a}_k) + \ell_T(\mathbf{x}_N) \quad (1a)$$

$$\text{s.t. } \mathbf{x}_0 = \hat{\mathbf{x}}_0, \quad (1b)$$

$$\mathbf{x}_{k+1} = f(\mathbf{x}_k, \mathbf{u}_k, \mathbf{a}_k), \quad k \in \mathbb{I}_0^{N-1}, \quad (1c)$$

$$h(\mathbf{x}_k, \mathbf{u}_k, \mathbf{a}_k) \leq 0, \quad k \in \mathbb{I}_0^{N-1}, \quad (1d)$$

where,  $\ell: \mathbb{R}^{n_x} \times \mathbb{R}^{n_u} \times \mathbb{R}^{n_a} \rightarrow \mathbb{R}$  is the stage cost function;  $\ell_T: \mathbb{R}^{n_x} \rightarrow \mathbb{R}$  is the terminal cost function. Initial condition (1b) is expressed by setting  $\mathbf{x}_0$  equal to the state estimate  $\hat{\mathbf{x}}_0$  received from the state estimator. The vector of model parameters  $\mathbf{a}_k$  is not optimized but is computed externally by the reference generator and provided to the optimization problem formulation. The nonlinear system dynamics are introduced by the equality constraints (1c). Finally, the path constraints are included with (1d) which, for example, can be bounds on the decision variables. The NLP (1) is defined for a time horizon  $T$  that is divided into  $N$  discrete time intervals of lengths  $T_s = \frac{T}{N}$ . Hereafter, we will refer to  $T_s$  as the *sampling time*, while we call  $N$  as *prediction horizon*.

### A. Cost

In our NMPC formulation we use a cost function of the form:

$$\ell(\mathbf{x}_k, \mathbf{u}_k, \mathbf{a}_k) = \|\mathbf{x}_k - \mathbf{x}_k^{\text{ref}}\|_{\mathbf{Q}}^2 + \|\mathbf{u}_k - \mathbf{u}_k^{\text{ref}}\|_{\mathbf{R}}^2 \quad (2a)$$

$$+ \|\mathcal{C}\mathbf{p}_{\text{hf}_k} - \mathcal{C}\mathbf{p}_{\text{hf}_k}^{\text{ref}}\|_{\mathbf{M}}^2 \quad (2b)$$

$$+ \rho \|\mathcal{K}\mathbf{u}_k\|_{\mathbf{P}}^2 \quad (2c)$$

where:

- The tracking cost (2a) is associated to state and control input and the references trajectories  $\mathbf{x}_k^{\text{ref}}, \mathbf{u}_k^{\text{ref}}$  are provided by the reference generator for each sampling instance  $k$  (refer Section V).
- The mobility cost (2b) is one of the contributions of this work that accounts for improving the leg mobility by penalizing the difference between the hip-to-foot relative position  $\mathcal{C}\mathbf{p}_{\text{hf}}$  and the reference value  $\mathcal{C}\mathbf{p}_{\text{hf}}^{\text{ref}}$  of maximum mobility. This cost allows the NMPC to optimize the robot base orientation (e.g. align it to the terrain) in order to increase the leg mobility of the robot without reaching the

kinematic limits during locomotion. The derivation of  $\mathcal{C}\mathbf{p}_{\text{hf}}^{\text{ref}}$  is detailed separately in Section IV-A.

- In some locomotion scenarios [4], to cope with uncertainties in the contact normal estimation and increase robustness to external disturbances, it is desirable to have the GRFs  $\mathbf{f}_i$  as close as possible to the center of the friction cone. This can be achieved by penalizing  $\mathbf{u}$  in a frame  $\mathcal{K}$  (see Fig. 3) that is aligned to the normal of the contact and it is included in our cost function by a control input regularization term (2c), refer Section IV-C for the details.

The positive definite weight matrices  $\mathbf{Q} \in \mathbb{S}_+^{n_x}, \mathbf{R} \in \mathbb{S}_+^{n_u}, \mathbf{M} \in \mathbb{S}_+^{12}, \mathbf{P} \in \mathbb{S}_+^{n_u}$  act as important tuning parameters in the NMPC formulation. The regularization factor  $\rho$  decides the trade-off between force robustness cost (2c) and both the tracking (2a) and mobility (2b) cost. Finally, we define the terminal cost  $\ell_T = \|\mathbf{x}_N - \mathbf{x}_N^{\text{ref}}\|_{\mathbf{Q}_N}$  and use the weight matrix  $\mathbf{Q}_N = \mathbf{Q}$  for this terminal cost.

### B. Robot Model

The inertial frame  $\mathcal{W}$  and the CoM frame  $\mathcal{C}$  are shown in Fig. 3. The CoM frame is aligned with the base of the robot and its origin is located at the CoM. A variable with left subscript denotes its frame of reference. For example  ${}_c\boldsymbol{\omega}$  represents the angular velocity of the robot base expressed in the CoM frame  $\mathcal{C}$ . Note that, unless explicitly specified, all the relevant quantities in this paper are defined in the inertial frame  $\mathcal{W}$ . Throughout this paper we define  $(a, \dots, b)$  as the column vector stacking any generic column vectors  $a, \dots, b$ .

We use a simplified reduced-order SRBD model [16] defined in a 6D space that describes the translational and angular dynamics of the robot while neglecting the dynamics of its legs. This is a valid approximation for the HyQ robot because most of its mass is concentrated in the base, as mentioned in [32] (mass of the base is 61.4 kg and mass of each leg is 6.5 kg). The robot is approximated as a rigid body with the inertia computed considering the robot in a default leg configuration as shown in Fig. 3. We choose to define the SRBD model in the CoM frame (specifically the angular dynamics) because this choice yields a constant inertia tensor. This allows our NMPC formulation to benefit from a lower computational complexity because the angular dynamic equations are much simpler i.e., less non-linear because the inertia tensor is not time varying and, consequently, less computationally demanding. In SRBD model, the GRFs are

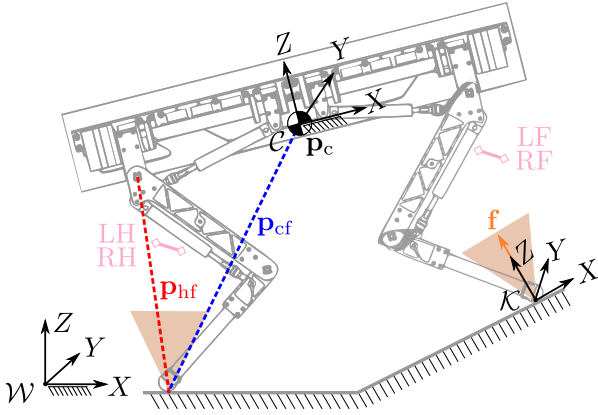


Fig. 3: HyQ schematic showing the inertial frame ( $\mathcal{W}$ ), the CoM frame ( $\mathcal{C}$ ) attached to the CoM of the robot, and the contact frame ( $\mathcal{K}$ ). The robot legs are shown in the *default* configuration.

applied as inputs to control the position and orientation of the robot base. The SRBD model is:

$$m\dot{\mathbf{v}}_c = m\mathbf{g} + \sum_{i=1}^4 \delta_i \mathbf{f}_i \quad (3a)$$

$${}^c\mathbf{I}_c c\dot{\boldsymbol{\omega}} + c\boldsymbol{\omega} \times {}^c\mathbf{I}_c c\boldsymbol{\omega} = \sum_{i=1}^4 \delta_i {}^c\mathbf{I}_{c,p_{cf,i}} \times c\mathbf{f}_i \quad (3b)$$

where  $m$  is the robot mass,  $\dot{\mathbf{v}}_c \in \mathbb{R}^3$  is the CoM acceleration,  $\mathbf{g}$  is the gravitational acceleration,  $\mathbf{f}_i \in \mathbb{R}^3$  is the ground reaction force of foot  $i$ ,  ${}^c\mathbf{I}_c \in \mathbb{R}^{3 \times 3}$  is the inertia tensor computed at the CoM frame origin,  $c\dot{\boldsymbol{\omega}} \in \mathbb{R}^3$  is the angular acceleration of the robot's base,  $\mathbf{p}_{cf,i} \in \mathbb{R}^3$  is the distance between the CoM position  $\mathbf{p}_c \in \mathbb{R}^3$  and the position  $\mathbf{p}_{f,i} \in \mathbb{R}^3$  of foot  $i$ . We introduce binary parameters  $\delta_i = \{0, 1\}$  to define whether foot  $i$  is in contact with the ground and can therefore generate contact forces or not.

The robot dynamics governed by (3) can be expressed as the continuous-time state-space model:

$$\begin{bmatrix} \dot{\mathbf{p}}_c \\ \dot{\mathbf{v}}_c \\ \dot{\boldsymbol{\Phi}} \\ c\dot{\boldsymbol{\omega}} \end{bmatrix} = \begin{bmatrix} \mathbf{v}_c \\ 1/m \sum_{i=1}^4 \delta_i \mathbf{f}_i + \mathbf{g} \\ \mathbf{E}'^{-1}(\boldsymbol{\Phi}) c\boldsymbol{\omega} \\ -c\mathbf{I}_c^{-1} (c\boldsymbol{\omega} \times {}^c\mathbf{I}_c) c\boldsymbol{\omega} + \sum_{i=1}^4 \delta_i {}^c\mathbf{I}_c^{-1} c\mathbf{p}_{cf,i} \times c\mathbf{f}_i \end{bmatrix} \quad (4)$$

where  $\mathbf{v}_c$  is the CoM velocity of the robot. The robot base orientation is represented by the vector of  $Z$ - $Y$ - $X$  Euler angles [38]  $\boldsymbol{\Phi} = (\phi, \theta, \psi)$  i.e., roll ( $\phi$ ), pitch ( $\theta$ ) and yaw ( $\psi$ ), respectively. The relation between the Euler Angles rates  $\dot{\boldsymbol{\Phi}}$  and angular velocity  $c\boldsymbol{\omega}$  is well-known and discussed in Appendix A for the sake of completeness. We define the state and control vectors as  $\mathbf{x} = (\mathbf{p}_c, \mathbf{v}_c, \boldsymbol{\Phi}, c\boldsymbol{\omega})$ , and  $\mathbf{u} = (\mathbf{f}_1, \dots, \mathbf{f}_4)$ . Equation (4) can be concisely written as:

$$\dot{\mathbf{x}}(t) = g(\mathbf{x}(t), \mathbf{u}(t), \mathbf{a}(t)), \quad (5)$$

where  $\mathbf{a} = (\mathbf{p}_f, \boldsymbol{\delta})$  is a vector of parameters that includes the feet positions  $\mathbf{p}_f$  and the contact sequences  $\boldsymbol{\delta} \in \mathbb{R}^4$ .

The rigid-body dynamics (5) are discretized using numerical integration [39, 40, 41, 42] to obtain the discrete-time model:

$$\mathbf{x}_{k+1} = f(\mathbf{x}_k, \mathbf{u}_k, \mathbf{a}_k), \quad (6)$$

which defines equality constraints (1c) imposed at every stage  $k$  in MPC to ensure that the state trajectory satisfies the system dynamics for the given control inputs.

One specific feature of legged robots is the need to ensure that the values of the GRFs equal to zero for a swinging leg. This is typically done by introducing complementarity constraints [31, 43]. These constraints, however, pose several difficulties in the solution of the optimization problem, since the vast majority of the NLP algorithms cannot handle them and tailored solvers are required. Ultimately, this results in a significant increase in computation time. An alternative to complementarity constraints consists in providing the contact sequences  $\boldsymbol{\delta}$  as input parameters in the state space model (5). In this manner, a contact mode  $\delta_i$  is multiplied with the terms involving force  $\mathbf{f}_i$  in (4) and the contribution of that force is nullified during the swing phase of the corresponding leg  $i$ . Hence, there is no more need to include complementarity constraints separately in (1) which results in fewer constraints and, consequently, in a relatively smaller NMPC formulation.

*Remark:* Note that Euler angles can suffer from singularities that occur in certain configurations [44]. Because in this work we do not consider motions that involve such configurations, using Euler angles does not pose any issue. A singularity-free implementation is out of the scope of this work and is left for future research.

### C. Friction cone and unilateral constraints

Friction cone constraints are encoded with their square pyramid approximation:

$$-\mu_i \underline{\mathbf{f}}_{z,i} \leq \mathbf{f}_{x,i} \leq \mu_i \underline{\mathbf{f}}_{z,i} \quad (7a)$$

$$-\mu_i \underline{\mathbf{f}}_{z,i} \leq \mathbf{f}_{y,i} \leq \mu_i \underline{\mathbf{f}}_{z,i} \quad (7b)$$

$$\underline{\mathbf{f}}_z \leq \mathbf{f}_{z,i} \leq \bar{\mathbf{f}}_z \quad (7c)$$

where,  $\underline{\mathbf{f}}_z$  and  $\bar{\mathbf{f}}_z$  are upper and lower bounds on GRFs  $Z$  component, respectively, and  $\mu_i$  is the friction coefficient of the contact surface. Choosing  $\underline{\mathbf{f}}_z$  greater than or equal to zero enforces unilateral constraints on the normal forces  $\mathbf{f}_z$ . The friction cone and unilateral constraint are represented by  $h(\mathbf{x}_k, \mathbf{u}_k, \mathbf{a}_k) \leq 0$  in the NMPC formulation.

## IV. LOCOMOTION-ENHANCING FEATURES

In this section we discuss the main distinctive features of our approach, which provide a quadruped robot with an enhanced locomotion ability. These features are *mobility*, *force robustness* and *kinematic robustness*.

### A. Mobility and Mobility Factor

A way to enable our NMPC to choose robot orientation adaptively to any terrain is to employ the concept of *mobility* [45]. In order to rigorously discuss mobility in mathematical terms, we first define it in words as the attitude of a manipulator (leg) to arbitrarily change end-effector position/orientation [46].

In order to penalize low leg mobility in the cost function (2b) we need to compute the reference value of hip-to-foot distance  $c\mathbf{p}_{hf}^{\text{ref}}$ . Our goal in this section is to define a convenient

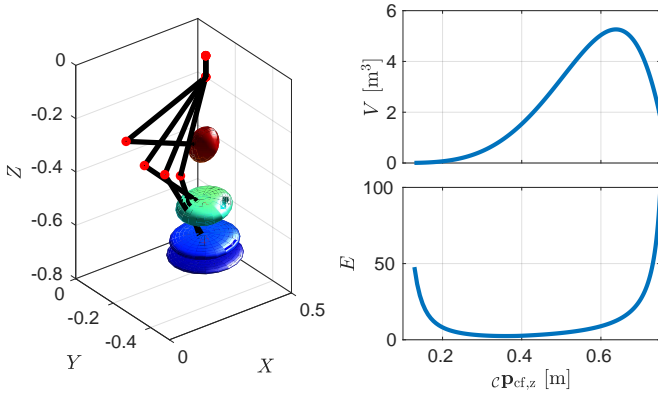


Fig. 4: Manipulability ellipsoid changing with leg configuration (left) of the right front leg. Volume of the ellipsoid (top right) and Eccentricity of the ellipsoid (bottom right).

metric to represent mobility and compute  $c\mathbf{p}_{\text{hf}_k}^{\text{ref}}$  corresponding to the maximum value of such a metric. Among several ways to compute mobility [45], the velocity transformation ratio [47] allows one to evaluate mobility in a particular direction. However, the velocity transformation ratio cannot be used in our setting because it requires prior knowledge of the evolution of the relative foot position with respect to CoM which is not available in advance in our case.

As an alternative approach, we consider the volume of the *manipulability ellipsoid* ( $\mathbf{v}(\mathbf{J}\mathbf{J}^T)^{-1}\mathbf{v} = 1$ ) [46] as a metric to evaluate mobility. A change in the volume of the manipulability ellipsoid with different leg configurations is visualized in Fig. 4 (left). Inspecting Fig. 4 (top right), it can be seen that the maximum volume  $V$  is in the vicinity of the most extended leg configuration because the mobility becomes very big in the  $X$  and  $Y$  direction, even if it is still very limited in the  $Z$  direction. However, because it is desirable to achieve a good mobility in all the directions of the leg configuration, a better metric to do so is the one that accounts for the *isotropy* of the manipulability ellipsoid. A measure of the isotropy of an ellipsoid can be expressed as the inverse of its *eccentricity*. Hence, a new manipulability index that we call *mobility factor* (8) can be defined in terms of both the eccentricity and the volume of manipulability ellipsoid. Again from Fig. 4, it can be visualized that to keep a good mobility (left plot) in all directions, the volume (top right plot) should be maximized while the eccentricity (bottom right plot) as small as possible. Defining a foot Jacobian  $\mathbf{J}(\mathbf{q}) \in \mathbb{R}^{3 \times 3}$  computed at a particular joint configuration  $\mathbf{q}$ , the volume  $V$  of a manipulability ellipsoid is evaluated as the product of the eigenvalues of  $(\mathbf{J}(\mathbf{q})\mathbf{J}(\mathbf{q})^T)^{-1}$  while the eccentricity is the ratio between its maximum and minimum eigenvalue [45]. First, the volume and eccentricity of manipulability ellipsoid are normalized by their ranges  $\bar{V}$  and  $\bar{E}$ . Then we define the mobility factor as:

$$l_m = \beta \frac{V}{\bar{V}} - \gamma \frac{E}{\bar{E}} \quad (8)$$

The minus sign in (8) represents conflicting contributions of the  $V$  and  $E$  in the definition of the mobility factor. Parameters

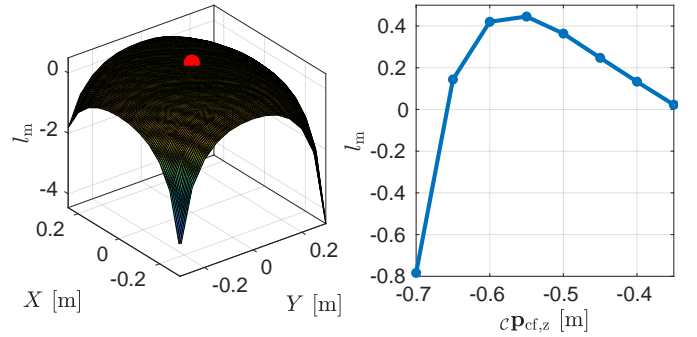


Fig. 5: Slices of the mobility factor function for the RF leg: the left figure plots it against the  $X$ - $Y$  components keeping  $Z$  constant. The red dot in the left plot represents the maxima. The right figure plots it against the  $Z$  component for a constant  $X$ - $Y$  foot position.

$\beta$  and  $\gamma$  are introduced to find a best trade-off between volume and eccentricity while deciding a mobility factor.

The mobility factor is a convex nonlinear function  $l_m : \mathbb{R}^3 \rightarrow \mathbb{R}$  that can be numerically evaluated inside the workspace of each leg. By selecting  $\beta = 1$  and  $\gamma = 4$ , and after conducting a numerical analysis for all the feet positions in the workspace of a leg of the HyQ robot we found that hip-to-foot distance  $c\mathbf{p}_{\text{hf}} = (0, 0, -0.55)$  m maximizes  $l_m$ . In Fig. 5 (left) we show a slice of the scalar function  $l_m$  in the  $X$ - $Y$  plane for  $c\mathbf{p}_{\text{hf},z} = -0.55$  m obtained for the Right-Front (RF) leg. Instead, in Fig. 5 (right) we plot  $l_m$  against the change of foot position in the  $Z$  direction considering the hip under the foot ( $X = 0, Y = 0$ ) which clearly highlights  $c\mathbf{p}_{\text{hf},z} = -0.55$  m corresponding to the maximum value of the mobility factor  $l_m$  (i.e., around 0.41). We use the output of this analysis as a reference for the hip-to-foot distance  $c\mathbf{p}_{\text{hf}}^{\text{ref}}$  in the mobility cost (2b) for all the legs.

In the mobility cost, we multiply  $\delta_i$  to the term corresponding to the  $i^{\text{th}}$  leg. Thus, the mobility cost solely accounts for stance legs because the robot can only use them to control its base orientation. Since, including the mobility cost enables NMPC to provide the optimal base orientation for a particular locomotion that retains mobility, there is no need to separately specify tracking cost for roll and pitch in the NMPC. This relieves a user from the burden of implementing a customized heuristic (e.g., to align the robot base to the terrain), as was necessary in, e.g., [3, 48, 43]. The relative tracking task for the CoM  $Z$  position is no longer required either, because maximizing the mobility in the  $Z$  direction automatically takes care of keeping an average distance of hips from the terrain to  $c\mathbf{p}_{\text{hf},z}$ , consequently keeping the robot base at a certain height.

Moreover, the yaw motion results by penalizing the mobility cost along the  $X$ - $Y$  directions. This has the effect of driving the hips of the robot base over the feet, naturally aligning the base to the feet, similar to what was done in [49]. However, a tracking cost on yaw was still necessary in the NMPC to avoid oscillations.

## B. Kinematic Robustness

In legged locomotion, the robot is often operated close to unstable configurations which require a controller to continuously compensate for model inaccuracies and external disturbances while maintaining locomotion stability. However, a configuration in which the Zero Moment Point (ZMP) [50] is close to the boundary of the support polygon [51] could cause instability even with small perturbations.

In our case, the reference generator computes references for the GRFs by dividing the robot mass with the number of legs as explained in Section V. Penalizing GRFs  $Z$  component heavily in the tracking cost (2a) ensures that they stay close to the reference, consequently maintaining a higher loading on the diagonally opposite leg to the swinging one, and therefore maintaining some margin for the locomotion stability. To evaluate the locomotion stability, we define the *ZMP margin* which is computed as the minimum of the distance of the ZMP from each support polygon edge, i.e.,

$$m_c = \min(\mathbf{d}) \quad (9)$$

where  $\mathbf{d}$  is a vector of the distances of ZMP projection from the support polygon edges.

## C. Force Robustness

Similar to the considerations on mobility, in order to effectively compensate for disturbances acting on the system, robustness in the GRFs is required. The closer the GRF is to the friction cone boundary, the less lateral force can be generated to compensate for perturbations. An approach penalizing GRFs that are in the vicinity of the cone boundaries has been proposed in [4, 5] inside the WBC. These WBC based approaches instantaneously generate GRFs that are as close as possible to the normals of the cones while yielding the prescribed resultant wrench on the robot base. However, WBC does not account for the future state of the robot and hence, it leaves some room for the NMPC to compensate for the contact normal estimation error and external disturbances. Introducing these margins on GRFs from the cone boundaries is especially important in some scenarios, such as the one reported in simulation in Section VIII-B2. In this paper, we adopt a similar idea to [4, 5] and introduce the additional cost term (2c) in the NMPC, which penalizes the tangential components of GRFs in the contact frame  $\mathcal{K}$  (see Fig. 3) to obtain the resultant GRFs as close as possible to the contact normals. The weight matrix  $\mathbf{P}$  used in this cost is defined in Table II (Section VIII).

## V. REFERENCE GENERATOR

In our approach, the NMPC requires a reference trajectory of the state and control input along with the model parameters i.e., foot positions and contact sequences. For the very first run of the NMPC, this reference trajectory also serves as an initial guess. The references are generated for the length of prediction horizon  $N$ , since the reference generator is called before every iteration of the NMPC in order to obtain prompt adaptation to terrain changes and user set-point. Our reference generator is based on heuristics and it takes as inputs:

- the user commanded longitudinal and lateral CoM velocity  ${}_{\mathcal{H}}\mathbf{v}_c^{\text{usr}} \in \mathbb{R}^2$  in the horizontal frame  $\mathcal{H}$ ,<sup>1</sup>
- user commanded heading velocity  $\omega_z^{\text{usr}} \in \mathbb{R}$ ,
- current pose of the robot  $(\mathbf{p}_c, \Phi)$ ,
- current feet positions  $\mathbf{p}_f \in \mathbb{R}^{12}$ ,
- heightmap of the terrain

The reference generator outputs:

- the references for the NMPC cost: states  $\mathbf{x}^{\text{ref}} \in \mathbb{R}^{N \times n_x}$ , control  $\mathbf{u}^{\text{ref}} \in \mathbb{R}^{N \times n_u}$ ,
- parameters  $\mathbf{a}$  of the model: contact sequences  $\delta \in \mathbb{R}^{N \times 4}$  and foot locations  $\mathbf{p}_f \in \mathbb{R}^{N \times 12}$ ,
- normals of the terrain at the foothold locations, which are provided as inputs to the NMPC for the cone constraints.

First we compute the  $X$ - $Y$  components of the total velocity  $\mathbf{v}_c^{\text{ref}} \in \mathbb{R}^3$  as the sum of  $\mathbf{v}_c^{\text{usr}}$  obtained by mapping  ${}_{\mathcal{H}}\mathbf{v}_c^{\text{usr}}$  in the world frame and the  $X$ - $Y$  components of the tangential velocity resulting from the angular rotation of the robot base due to heading velocity  $\omega^{\text{usr}} = (0, 0, \omega_z^{\text{usr}})$ .

$$\mathbf{v}_{c,(x,y)}^{\text{ref}} = \mathbf{v}_c^{\text{usr}} + (\omega^{\text{usr}} \times \mathbf{p}_c^{\text{ref}})_{(x,y)} \quad (10)$$

The  $X$ - $Y$  CoM position  $\mathbf{p}_{c,(x,y)}^{\text{ref}}$  is obtained by integrating the  $\mathbf{v}_{c,(x,y)}^{\text{ref}}$  with the explicit Euler scheme. The references for CoM  $Z$ , roll and pitch are set to 0 because we do not track them in the NMPC cost (2a). Instead, the reference for the yaw is obtained by integrating the user defined yaw rate  $\dot{\psi}^{\text{usr}}$ . To do so, first  $\dot{\Phi}^{\text{usr}}$  is computed from the heading velocity as explained in Appendix A:  $\dot{\Phi}^{\text{usr}} = \mathbf{E}^{-1}(\Phi^{\text{ref}})\omega^{\text{usr}}$  and then yaw rate is extracted from this vector. Therefore, the equation that represents the heuristics to update the state references is:

$$\mathbf{x}_{k+1}^{\text{ref}} = \left( \mathbf{p}_{c_{k+1}}^{\text{ref}}, \mathbf{v}_{c_{k+1}}^{\text{ref}}, \Phi_{k+1}^{\text{ref}}, \omega_{k+1}^{\text{ref}} \right) \quad (11)$$

where,  $\mathbf{p}_{c_{k+1}}^{\text{ref}} = (\mathbf{p}_{c_{k,(x,y)}}^{\text{ref}} + T_s \mathbf{v}_{c_{k,(x,y)}}^{\text{ref}}, 0)$ ,  $\mathbf{v}_{c_{k+1}}^{\text{ref}} = (\mathbf{v}_c^{\text{usr}} + (\omega^{\text{usr}} \times \mathbf{p}_{c_k}^{\text{ref}})_{(x,y)}, 0)$ ,  $\Phi_{k+1}^{\text{ref}} = (0, 0, \psi_k^{\text{ref}}) + T_s(0, 0, \dot{\psi}^{\text{usr}})$  and  $\omega_{k+1}^{\text{ref}} = \omega^{\text{usr}}$ . The references for GRFs  $\mathbf{u}^{\text{ref}}$  are calculated by simply dividing the total mass of the robot by the number of legs in stance.

The contact sequences  $\delta$  and footholds are computed by the *gait scheduler* and *robocentric stepping*, respectively. It is important to mention that the reference generator does not compute the swing trajectories and they are obtained from the WBC interface discussed in Section VI-A.

1) *Gait scheduler*: The gait scheduler is logically decoupled from the generation of reference trajectories and determines if each leg is either in swing or in stance ( $\delta_i$ ) at each time instance for the entire gait cycle as shown in Fig. 6 (left).

The leg duty factor  $D_i$  and offsets  $o_i$  can be used to encode different gaits such as crawl, trot and pace. The gait scheduler implements a time parametrization  $s$  (*stride phase*) which is normalized about the cycle time duration  $T_c$  such that the leg duty factor  $D_i$  and offsets  $o_i$  are independent from the cycle time. Time parametrization  $s$  is reset at the end of each cycle

<sup>1</sup>The horizontal frame is placed like the CoM frame but with the  $Z$ -axis aligned with the gravity

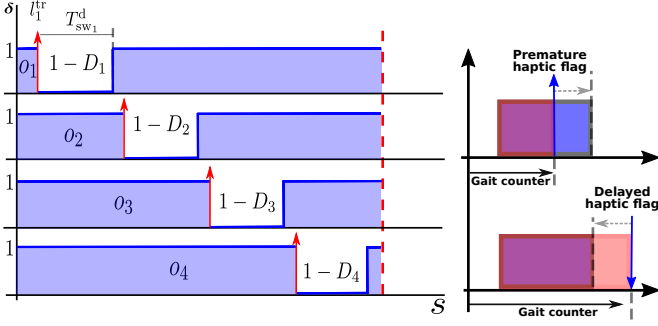


Fig. 6: Gait schedule for walk. Offsets  $\mathbf{o} = [0.05, 0.3, 0.55, 0.8]$ , duty-factors  $\mathbf{D} = [0.85, 0.85, 0.85, 0.85]$ . The red arrows represent the triggers  $l_i^{\text{tr}}$  for the swing legs. Right part shows the fast-forwarding or the re-winding of the gait counter to recover synchronization between actual (haptic) and planned touchdown.

resulting in a sawtooth pattern. Once we have defined  $s$ , we can express the value of  $\delta$  for leg  $i$  as

$$\delta_i = \begin{cases} 1, & (s < o_i) \vee s > (o_i + (1 - D_i)) \\ 0, & \text{otherwise} \end{cases} \quad (12)$$

Changing the gait cycle duration changes the slope of  $s$  resulting in different frequencies of the swing events. The gait scheduler also computes the default swing duration,  $T_{\text{sw}_i}^{\text{d}}$  according to the duty factor  $D_i$ . Note that since the gait schedule of leg  $i$  is normalized between 0 and 1, to recover the real swing duration  $T_{\text{sw}}^{\text{d}}$  one needs to multiply it by the cycle duration  $T_c$ . Each trigger  $l_i^{\text{tr}}$  corresponds to a new lift-off event. Every time the reference generator is called, it extracts  $N$  points from the gait schedule obtaining the contact sequence for the entire prediction horizon (that could last also more than one gait cycle), starting from an index called *gait counter* that keeps *memory* of the index of the gait schedule achieved by the previous call of the reference generator. The synchronization between the first point of a contact sequence  $\delta_{i_k}$  computed by the reference generator and the actual contact state of the robot is crucial for locomotion. This is to avoid the reference generator to compute a zero reference force while the leg is in stance and vice-versa. In the case of premature or delayed touchdown events on uneven terrains this synchronization is lost. To recover the synchronization, it is possible to shift the gait counter backwards or forward to re-conciliate the planned touchdown with the actual touchdown as shown in Fig. 6 (right).

2) *Robocentric stepping*: The choice of the foothold is a key element in locomotion, since it deals with the kinematic limits of the robot. We use an approach that continuously computes footholds consistent with the current position of the robot. To compute a foothold for the swinging leg  $i$ , we consider its hip position  $\mathbf{h}_i$  instead of using the foot position at the moment of lift-off. In this way a disturbance acting on the robot or a tracking error occurred during a swing can be recovered in the following swing. For a leg  $i$ , dropping the index to simplify the notation and defining the lift-off trigger

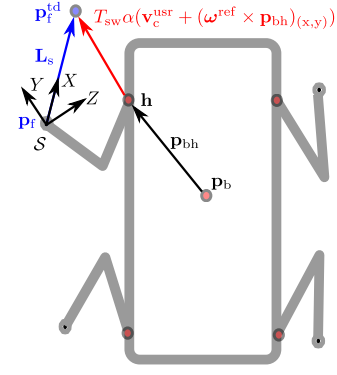


Fig. 7: Representation of the robocentric stepping strategy and of the Swing Frame, located at the lift-off point. The red arrow shows the distance between the touchdown point  $\mathbf{p}_f^{\text{td}}$  and the hip  $\mathbf{h}$ . The blue vector  $\mathbf{L}_{\text{sw}}$  connects lift-off and touchdown point.

as  $l_k^{\text{tr}} = \delta_k \wedge \bar{\delta}_{k+1}$ , the foot position is computed as:

$$\mathbf{p}_{f_{k+1}} = \begin{cases} \mathbf{p}_{f_k}^{\text{td}} & l_k^{\text{tr}} = 1 \\ \mathbf{p}_{f_k} & l_k^{\text{tr}} = 0 \end{cases} \quad (13)$$

We can notice that at the lift-off condition  $l^{\text{tr}} = 1$  at instance  $k$ ,  $\mathbf{p}_f$  is set equal to the touchdown point  $\mathbf{p}_f^{\text{td}}$  and it is kept constant until the next lift-off event occurs. The X-Y component of the touchdown point is given by

$$\mathbf{p}_{f_k, (x,y)}^{\text{td}} = \mathbf{h}_k + T_{\text{sw}}^{\text{d}}\alpha(\mathbf{v}_c^{\text{usr}} + (\boldsymbol{\omega}^{\text{usr}} \times \mathbf{p}_{\text{bh}})_{(x,y)}) \quad (14)$$

where  $\mathbf{h}_k = \mathbf{p}_{b_k, (x,y)}^{\text{ref}} + \mathbf{p}_{\text{bh}, (x,y)}$  is the X-Y components of the hip position,  $\mathbf{p}_{b_k}^{\text{ref}} \in \mathbb{R}^3$  is the position of the geometric center of the base<sup>1</sup> and  $\mathbf{p}_{\text{bh}} \in \mathbb{R}^3$  is the distance between hip and center of the base. The second term in (14) represents the step length (red arrow in Fig. 7) which is computed with respect to the hip (non the previous foot location) so that the foot velocity incorporates the desired base velocity from the user. Parameter  $\alpha$  is a scaling factor between foot and CoM velocity chosen empirically, and the term  $\boldsymbol{\omega}^{\text{usr}} \times \mathbf{p}_{\text{bh}}$  is the contribution of  $\boldsymbol{\omega}^{\text{usr}}$  to the foot velocity. A 2.5D heightmap of the terrain is evaluated in correspondence of the touchdown point  $\mathbf{p}_{f_k, (x,y)}^{\text{td}}$  to obtain a  $\mathbf{p}_{f_k, z}^{\text{td}}$  that does not penetrate the terrain.

3) *Vision-based Foothold Adaptation (VFA)*: The robocentric stepping provides a touchdown location  $\mathbf{p}_f^{\text{td}}$  that is coherent with the terrain. However, if  $\mathbf{p}_f^{\text{td}}$  is located near an edge or leads to collisions (e.g., of the foot or the shin) during the step cycle, this can be harmful for the robot's balance. To prevent this from happening, we integrated the VFA module presented in [52], which works as follows. The robot acquires a local heightmap in the vicinity of the touchdown location  $\mathbf{p}_f^{\text{td}}$  extracting it from the full 2.5D heightmap surrounding the robot. The local heightmap corresponds to a  $15 \times 15$  grid centered at  $\mathbf{p}_f^{\text{td}}$  with a resolution of 4 cm. The VFA adjusts the foot landing location to avoid collisions, sharp edges, narrow gaps/holes, and footholds that are outside the workspace of the swinging leg. This module uses a pre-trained

<sup>1</sup>In order to compute  $\mathbf{p}_{b_k}^{\text{ref}}$  we assume that its velocity is equal to the one of the CoM, so  $\mathbf{p}_{b_k, (x,y)}^{\text{ref}} = \mathbf{p}_{b_{k-1}, (x,y)}^{\text{ref}} + T_s \mathbf{v}_c^{\text{ref}}$

Convolutional Neural Network (CNN) that takes as input the  $15 \times 15$  local heightmap and outputs an adjustment for the touchdown location  $\mathbf{p}_f^{\text{td}}$  within the local heightmap. The CNN has low computational time ( $\approx 0.2$  ms per adjustment), which allows the robot to adapt the landing location of the feet without compromising the computation of the control action provided by the NMPC. Details on how the CNN is trained can be found in [52].

## VI. WHOLE-BODY CONTROLLER

In this section, we describe the WBC that tracks planned trajectories  $\mathbf{x}^{\text{p}}$  and  $\mathbf{u}^{\text{p}}$  provided by the NMPC. The WBC first computes feed-forward  $\mathbf{W}_{\text{ff}}^{\text{d}}$  and feedback  $\mathbf{W}_{\text{fb}}^{\text{d}}$  wrenches from the planned trajectories and then the sum of these wrenches are mapped into GRFs through the QP optimization (21). The WBC also maps the GRFs into the joint torques  $\boldsymbol{\tau}^*$ . This joint torque along with low-impedance feedback torque  $\boldsymbol{\tau}_{\text{fb}}$  results in the total torque  $\boldsymbol{\tau}_{\text{d}}$  required by the low-level joint torque control block. Refer to Fig. 2 for the block representation of WBC inside our locomotion framework.

### A. WBC interface

In our planning framework, the NMPC runs at 25 Hz which we will refer to as *re-planning frequency* whereas the WBC requires state and control inputs at 250 Hz (we will call this the *WBC frequency*). Hence, we introduce a WBC interface block that re-samples state and control inputs at the WBC frequency. Furthermore, the WBC interface takes care of generating the swing trajectory connecting subsequent footholds and managing the premature/delayed touchdowns. Particularly, the WBC interface provides the desired state  $\mathbf{x}^{\text{d}}$ , desired GRFs  $\mathbf{u}^{\text{d}}$ , joint position  $\mathbf{q}^{\text{d}}$ , joint velocity  $\dot{\mathbf{q}}^{\text{d}}$  and feed forward wrenches  $\mathbf{W}_{\text{ff}}^{\text{d}}$  at any given time instant.

1) *Re-sampling*: In order to obtain the desired  $\mathbf{u}^{\text{d}}$  at WBC frequency we use a zero-order hold. At a certain sampling instance  $k$ , the value of  $\mathbf{u}^{\text{d}}$  between interval  $i$  and  $i + 1$  is kept equal to the value of  $\mathbf{u}^{\text{p}}$  obtained at the instance  $k$ ,

$$\mathbf{u}_{k,i}^{\text{d}} = \mathbf{u}_k^{\text{p}}, \quad i \in \mathbb{I}_0^{f_r-1} \quad (15)$$

where  $f_r \in \mathbb{R}$  is the ratio between the WBC frequency and re-planning frequency. Moreover, the planned states  $\mathbf{x}^{\text{p}}$  from the NMPC are re-sampled with a linear interpolation to obtain  $\mathbf{x}^{\text{d}}$  at the WBC frequency<sup>1</sup>:

$$\mathbf{x}_{k,i}^{\text{d}} = \mathbf{x}_k^{\text{p}} + i \frac{\mathbf{x}_{k+1}^{\text{p}} - \mathbf{x}_k^{\text{p}}}{f_r}, \quad i \in \mathbb{I}_1^{f_r} \quad (16)$$

2) *Joint trajectory generation*: To compute the joint trajectories, inverse kinematics is required which in turn needs the swing trajectory  $\mathbf{p}_f^{\text{sw}}$ . The latter substitutes the constant foot position  $\mathbf{p}_f$  computed by the reference generator for a swinging leg i.e., when  $\delta_i = 0$ . We define the swing frame  $\mathcal{S}$  [49], whose  $X$ -axis is aligned with the vector that links lift-off and touchdown point ( $\mathbf{L}_{\text{sw}}$ ),  $Y$ -axis is perpendicular

to the  $X$ -axis of the swing frame and to the  $Z$ -axis of the world frame. Finally the  $Z$ -axis is such that  $\mathcal{S}$  is a counter-clockwise coordinate system. The origin of the swing frame  $\mathcal{S}$  coincides with the lift-off point, see Fig. 7. In this way the swing trajectory lies on the  $X$ - $Z$  plane and we shape it as a semi-ellipse with  $L_{\text{sw}}$  and  $H_{\text{sw}}$  as length of the axes:

$${}_{\mathcal{S}}\mathbf{p}_f^{\text{sw}} = \begin{bmatrix} \frac{L_{\text{sw}}}{2}(1 - \cos(\pi f_{\text{sw}} t_{\text{sw}})) \\ 0.0 \\ H_{\text{sw}} \sin(\pi f_{\text{sw}} t_{\text{sw}}) \end{bmatrix} \quad (17)$$

where  $t_{\text{sw}}$  is the time elapsed from the beginning of a swing and  $f_s = 1/T_{\text{sw}}$  is the swing frequency computed from user-defined cycle time and the duty cycle of a leg. We map  ${}_{\mathcal{S}}\mathbf{p}_f^{\text{sw}}$  in the inertial frame  $\mathcal{W}$  to obtain  $\mathbf{p}_f^{\text{sw}}$ . Similarly, the foot velocity is computed as the derivative of  ${}_{\mathcal{S}}\mathbf{p}_f^{\text{sw}}$  and then mapped to  $\mathcal{W}$ . Finally, after evaluating the relative foot position  ${}_{\mathcal{C}}\mathbf{p}_{\text{cf}}$  and velocity  ${}_{\mathcal{C}}\dot{\mathbf{p}}_{\text{cf}}$  we can obtain  $\mathbf{q}^{\text{d}}$  and  $\dot{\mathbf{q}}^{\text{d}}$  via inverse kinematics.

3) *Feed-forward wrench*: The feed-forward wrench  $\mathbf{W}_{\text{ff}} \in \mathbb{R}^6$  is computed from the desired GRFs  $\mathbf{u}^{\text{d}}$  as,

$$\mathbf{W}_{\text{ff}}^{\text{d}} = \left[ \sum_{i=1}^4 \mathbf{u}_i^{\text{d}} \quad \sum_{i=1}^4 \mathbf{p}_{\text{cf},i}^{\text{d}} \times \mathbf{u}_i^{\text{d}} \right]^{\top} \quad (18)$$

### B. Feedback wrench

Since most of the mass of HyQ is located in its base, the average angular velocity of the robot is assumed to be equal to the angular velocity of the base. We use the approach of [4] to define desired feedback wrench obtained from a Cartesian impedance and briefly recall it next for completeness:

$$\mathbf{W}_{\text{fb}}^{\text{d}} = \mathbf{K} \begin{bmatrix} \mathbf{p}_c^{\text{d}} - \mathbf{p}_c \\ \mathbf{e}_{(\text{w}\mathbf{R}_b^{\top} \text{w}\mathbf{R}_d)} \end{bmatrix} + \mathbf{D} \begin{bmatrix} \mathbf{v}_c^{\text{d}} - \mathbf{v}_c \\ \boldsymbol{\omega}_b^{\text{d}} - \boldsymbol{\omega}_b \end{bmatrix} \quad (19)$$

where  $\mathbf{p}_c^{\text{d}}$ , and  $\mathbf{v}_c^{\text{d}}$  and  $\boldsymbol{\omega}_b^{\text{d}} \in \mathbb{R}^3$  are the desired CoM position, CoM velocity and angular velocity of the base. Matrices  ${}_{\text{w}}\mathbf{R}_b$  and  ${}_{\text{w}}\mathbf{R}_d \in \mathbb{R}^{3 \times 3}$  are the rotation matrices representing actual and desired orientation of the base with respect to the inertial frame, respectively,  $\mathbf{e}(\cdot) : \mathbb{R}^{3 \times 3} \rightarrow \mathbb{R}^3$  is a mapping from a rotation matrix to the associated rotation vector, composed of the three off-diagonal terms in the (skew-symmetric) matrix logarithm of the argument. Matrices  $\mathbf{K}$  and  $\mathbf{D}$  are diagonal matrices containing the proportional and derivative gains and they can be interpreted as impedances.

*Remark*: At each re-planning instance of NMPC, the state reference is computed from the current state of the robot  $\hat{\mathbf{x}}_0$ . Thus, at each re-planning instance the feedback term is nullified.

### C. Projection of the GRFs

While the feedforward wrenches  $\mathbf{W}_{\text{ff}}^{\text{d}}$  provided by MPC satisfy the friction cone and unilateral constraints by construction, this guarantee is lost with the addition of the feedback term  $\mathbf{W}_{\text{fb}}^{\text{d}}$  to the wrenches. Therefore, one needs to project the total wrenches  $\mathbf{W}_{\text{ff}}^{\text{d}} + \mathbf{W}_{\text{fb}}^{\text{d}}$  onto the set of wrenches that satisfy the constraints. The matrix representation

$$\underbrace{\begin{bmatrix} \delta_1 \mathbf{I} & \dots & \delta_e \mathbf{I} \\ \delta_1 [\mathbf{p}_{\text{cf},1} \times] & \dots & \delta_e [\mathbf{p}_{\text{cf},e} \times] \end{bmatrix}}_{\mathbf{A}} \underbrace{\begin{bmatrix} \mathbf{f}_1 \\ \vdots \\ \mathbf{f}_e \end{bmatrix}}_{\mathbf{f}} = \underbrace{\mathbf{W}_{\text{ff}}^{\text{d}} + \mathbf{W}_{\text{fb}}^{\text{d}}}_{\mathbf{b}} \quad (20)$$

<sup>1</sup>The rigorous approach is to use the model (3) to predict the evolution of the system in the  $T_s$  time interval, considering the  $\mathbf{u}^{\text{p}}$  coming from the NMPC, but for the motions considered in this paper the result is very similar, so a linear interpolation is a fair approximation.

is derived from a simplified SRBD model [4] and allows us to map the desired wrenches into GRFs. To compute the desired GRFs  $\mathbf{f}^d$  we solve the following QP:

$$\mathbf{f}^d = \underset{\mathbf{f}}{\operatorname{argmin}} \quad \|\mathbf{A}\mathbf{f} - \mathbf{b}\|_{\mathbf{S}}^2 + \|\mathbf{f} - \mathbf{u}^d\|_{\mathbf{T}}^2 \quad (21a)$$

$$\text{s.t.} \quad \underline{\mathbf{d}} \leq \mathbf{C}\mathbf{f} \leq \bar{\mathbf{d}} \quad (21b)$$

The term  $\|\mathbf{f} - \mathbf{u}^d\|_{\mathbf{T}}^2$  in the cost (21) allows the tracking of the desired forces  $\mathbf{u}^d$  received from the NMPC. This term is required because the information on the specific direction of the GRFs is lost when projected into the lower dimensional 6D wrench space in (18). Matrices  $\mathbf{S} \in \mathbb{S}_+^6$  and  $\mathbf{T} \in \mathbb{S}_+^{12}$  are positive-definite weight matrices. Inequality (21b) encodes the friction cone and unilateral constraints similar to (7) for which further details can be found in [4]. It is important to note that in (20) we do not need to include gravity compensation because it is already incorporated in the NMPC formulation through the SRBD model.

### D. Mapping GRFs to Joint Torques

Since the real actuators apply torques to the leg joints, the GRFs  $\mathbf{f}^d$  must be mapped into joint torques  $\boldsymbol{\tau}^*$ . We do so by exploiting the kinematic relation:

$$\boldsymbol{\tau}^* = -\mathbf{J}(\mathbf{q})^\top \mathbf{f}^d + \mathbf{h}(\mathbf{q}, \dot{\mathbf{q}}) \quad (22)$$

where  $\mathbf{J}(\mathbf{q}) \in \mathbb{R}^{n_u \times n_x}$  is the contact Jacobian and  $\mathbf{h}(\mathbf{q}, \dot{\mathbf{q}})$  the vector of gravity/Coriolis terms in the leg dynamics.

*Remark:* A 1kHz Joint-Space PD is put in cascade with the WBC before sending torques to the low-level controller. In this way, we track the desired trajectories of the swing legs and we increase the robustness in case a foot loses contact with the ground.

## VII. RTI FOR NMPC

One of the main drawbacks of NMPC is its computational burden, thus efficient tailored algorithms are necessary in order to achieve fast sampling rates for complex systems with fast dynamics. While many approaches have been developed for optimal control, a complete discussion about all possible approaches is beyond the scope of this paper. We focus on direct multiple shooting using methods derived from Sequential Quadratic Programming (SQP) that have been specifically developed for real-time NMPC [33].

In multiple shooting methods both state  $\mathbf{x}$  and control input  $\mathbf{u}$  are decision variables unlike in single shooting where the decision vector only includes the control input. We ought to stress that this does not increase the computational complexity with respect to single shooting (where computations are moved from linear algebra to the evaluation of derivatives); on the contrary, it allows one to use tailored sparse linear algebra, which can actually reduce the computational burden. Furthermore, multiple-shooting allows one to provide an initial guess also for the state trajectory, which is typically beneficial for unstable systems in an NMPC context [33].

SQP is a popular algorithm which solves an NLP by iteratively solving local quadratic approximations (QPs) of the problem [34]. At each SQP iteration, the solution from the

previous step is recycled to define an initial guess  $(\mathbf{x}_k^L, \mathbf{u}_k^L)$ , which is then used to construct a QP approximation of the NLP (1), given by

$$\min_{\Delta \mathbf{x}, \Delta \mathbf{u}} \quad \sum_{k=0}^{N-1} \frac{1}{2} \begin{bmatrix} \Delta \mathbf{x}_k \\ \Delta \mathbf{u}_k \end{bmatrix}^\top \mathbf{H}_k \begin{bmatrix} \Delta \mathbf{x}_k \\ \Delta \mathbf{u}_k \end{bmatrix} + \mathbf{J}_k^\top \begin{bmatrix} \Delta \mathbf{x}_k \\ \Delta \mathbf{u}_k \end{bmatrix} \quad (23a)$$

$$\text{s.t.} \quad \Delta \mathbf{x}_0 = \hat{\mathbf{x}}_0 - \mathbf{x}_0^L, \quad (23b)$$

$$\Delta \mathbf{x}_{k+1} = \mathbf{A}_k \Delta \mathbf{x}_k + \mathbf{B}_k \Delta \mathbf{u}_k + \mathbf{r}_k, \quad (23c)$$

$$\mathbf{C}_k \Delta \mathbf{x}_k + \mathbf{D}_k \Delta \mathbf{u}_k + \mathbf{h}_k \geq 0, \quad (23d)$$

where,  $\Delta \mathbf{x}_k = \mathbf{x}_k - \mathbf{x}_k^L$ ,  $\Delta \mathbf{u}_k = \mathbf{u}_k - \mathbf{u}_k^L$ ,  $\hat{\mathbf{x}}_0$  is the current system state, and

$$\begin{aligned} \mathbf{A}_k &= \left. \frac{\partial f(\mathbf{x}, \mathbf{u}, \mathbf{a}_k)}{\partial \mathbf{x}} \right|_{\mathbf{x}_k^L, \mathbf{u}_k^L}, & \mathbf{B}_k &= \left. \frac{\partial f(\mathbf{x}, \mathbf{u}, \mathbf{a}_k)}{\partial \mathbf{u}} \right|_{\mathbf{x}_k^L, \mathbf{u}_k^L}, \\ \mathbf{C}_k &= \left. \frac{\partial h(\mathbf{x}, \mathbf{u}, \mathbf{a}_k)}{\partial \mathbf{x}} \right|_{\mathbf{x}_k^L, \mathbf{u}_k^L}, & \mathbf{D}_k &= \left. \frac{\partial h(\mathbf{x}, \mathbf{u}, \mathbf{a}_k)}{\partial \mathbf{u}} \right|_{\mathbf{x}_k^L, \mathbf{u}_k^L}, \\ \mathbf{r}_k &= g(\mathbf{x}_k^L, \mathbf{u}_k^L, \mathbf{a}_k) - \mathbf{x}_{k+1}^L, & \mathbf{h}_k &= h(\mathbf{x}_k^L, \mathbf{u}_k^L, \mathbf{a}_k) \\ \mathbf{J}_k &= \mathbf{W}_k \begin{bmatrix} \mathbf{x}_k^L - \mathbf{x}_k^{\text{ref}} \\ \mathbf{u}_k^L - \mathbf{u}_k^{\text{ref}} \end{bmatrix} \end{aligned} \quad (24)$$

Matrix  $\mathbf{H}_k$  is the diagonal blocks of a suitable approximation of the Lagrangian Hessian. Since our problem relies on a least-squares cost, we adopt the popular Gauss-Newton Hessian approximation [34] that gives  $\mathbf{H}_k = \mathbf{W}_k$ . Matrix  $\mathbf{W}_k$  is equal to the  $\operatorname{diag}(\mathbf{Q}, \mathbf{R}, \mathbf{M}, \mathbf{P})$ .

While in SQP one solves several QPs until convergence is reached, the RTI scheme consists in solving a single QP per sampling time. This is motivated by the observation that in NMPC two subsequent problems have very similar solutions. Therefore, by reusing the solution of the previous NMPC problem, one obtains a very good initial guess for the next problem, which essentially only needs to correct for external perturbations and model mismatch. For all details on the RTI scheme, we refer to [26, 34] and references therein. We limit ourselves to observe that, since  $(\mathbf{x}_k^L, \mathbf{u}_k^L)$  is known *before* the next state measurement is available, one can already evaluate the functions and their derivatives (24) before the initial state  $\hat{\mathbf{x}}_0$  is available. Consequently, the QP can be constructed and prepared beforehand; note that this also includes the first factorization of the QP Hessian. Once  $\hat{\mathbf{x}}_0$  is available, one only has to finish solving the QP. Therefore, while the overall sampling time must still be long enough to prepare the next QP, the latency between the time at which  $\hat{\mathbf{x}}_0$  is available and the time at which the control input can be applied to the system is very small.

Note that in the RTI scheme proposed above, the functions and their derivatives (24) are evaluated along a guess obtained from the previous solution, rather than along the reference trajectory. Another important aspect to highlight is the fact that there exist several approaches to compute (24). One choice consists of first linearizing the continuous-time system dynamics and then using the matrix exponential to obtain a discrete-time linear system. This approach presents some advantages, but can be computationally demanding. For the time-varying and infeasible references, however, it is preferred

to *first discretize and then linearize* [34]. In this work we deal with time-varying and infeasible references, hence we opt for first discretize and then linearize approach. An advantage of this approach is that after numerically approximating the discrete-time dynamics, the linearization can be obtained at a desired accuracy.

A very popular way to obtain discrete-time dynamics is with the explicit Euler integrator, which is computationally inexpensive, but can be inaccurate and unstable. Therefore, it is usually more efficient to resort to higher-order integration schemes, such as, e.g., the popular Runge-Kutta methods. Finally, we should further stress that there also exist implicit integration schemes, which require more computations per step, but they are typically much more stable and accurate than explicit schemes for some classes of systems. Unfortunately, the selection of the least computationally demanding integrator which delivers sufficient accuracy depends on the problem setting and typically requires some trial-and error approach, which can be educated using some guidelines based on the theoretical properties of each integrator [39, 53, 41, 42, 40].

In this work, we relied on the RTI implementation provided by *acados* [27], which consists of tailored efficient implementations of QP solvers, numerical integration schemes, and all other components of the RTI scheme.

## VIII. RESULTS

In this section we discuss the implementation details and results obtained from the simulations and experiments with the NMPC scheme proposed in section III.

### A. Implementation details

To check the efficacy of our RTI based NMPC algorithm with the proposed features mentioned in Section IV, we performed several simulations and experiments in challenging scenarios. The simulation and experiments were performed on the HyQ robot of mass  $m = 87.4$  kg and inertia  $c\mathbf{I}_c$  ( $I_{xx} = 4.0745$ ,  $I_{xy} = 0.1458$ ,  $I_{xz} = -0.2245$ ,  $I_{yy} = 11.3576$ ,  $I_{yz} = -0.0133$ ,  $I_{zz} = 12.5675$ ). The feedback gains used in the WBC are  $\mathbf{K} = \text{diag}(1500, 1500, 1500, 100, 100, 100)$  and  $\mathbf{D} = \text{diag}(1000, 1000, 1000, 50, 50, 50)$ . We chose the weights  $\mathbf{S} = \text{diag}(5, 5, 10, 10, 10, 10)$  and  $\mathbf{T} = \text{diag}(1000, \dots, 1000)$  for the QP (21). The parameters and weights used by the NMPC are reported in Table I and II, respectively. In all of our simulations and experiments, we do not set any weights on the CoM  $X$ - $Y$ , roll ( $\phi$ ) and pitch ( $\theta$ ) tasks because we wanted the NMPC to sort out these CoM trajectories autonomously.

1) *Discretization*: For the discretization of the dynamic constraints, we mainly investigated two integration schemes, i.e., a single step of the explicit and implicit Euler, both of order 1 due to their low computational complexity that favors our real-time implementation needs. We compared the accuracy of these single-step first-order integration schemes with more accurate integration schemes and verified that our results were accurate enough for the purpose of our control task. We chose the implicit Euler integration scheme of order 1 because of its stability and accuracy properties. The sampling time  $T_s = 40$  ms was chosen and it was sufficient to conduct

TABLE I: NMPC parameters

Parameter	Symbol	Value	Unit
Number of state	$n_x$	12	-
Number of control inputs	$n_u$	12	-
Number of model parameters	$n_a$	16	-
Time horizon	$T$	2	s
Sampling time	$T_s$	0.04	s
Prediction horizon	$N$	50	-
Friction coefficient	$\mu$	0.7	-
GRFs lower bound	$\underline{\mathbf{f}}_z$	0	N
GRFs upper bound	$\bar{\mathbf{f}}_z$	500	N
Hip-to-foot position reference	$c\mathbf{P}_{\text{hf},i}^{\text{ref}}$	(0.0, 0.1, -0.55)	m
Regularization parameter	$\rho$	$3 \times 10^{-5}$	-

TABLE II: Weights used in NMPC

Cost	Weight	Value
State	$\mathbf{Q}_{\mathbf{p}_c}$	$\text{diag}(0, 0, 0)$
	$\mathbf{Q}_{\mathbf{v}}$	$\text{diag}(100, 100, 100)$
	$\mathbf{Q}_{\boldsymbol{\phi}}$	$\text{diag}(0, 0, 100)$
	$\mathbf{Q}_{\boldsymbol{\omega}}$	$\text{diag}(100, 100, 1000)$
Force	$\mathbf{R}_x$	$1 \times 10^{-3}$
	$\mathbf{R}_y$	$1 \times 10^{-3}$
	$\mathbf{R}_z$	$8 \times 10^{-4}$
Mobility	$\mathbf{M}_x$	$1 \times 10^{-4}$
	$\mathbf{M}_y$	$2 \times 10^{-3}$
	$\mathbf{M}_z$	1000
Force robustness	$\mathbf{P}_x$	100
	$\mathbf{P}_y$	100
	$\mathbf{P}_z$	1

NMPC computation *online* along with the other necessary computations for the re-planning.

2) *NMPC software*: We use the *acados* software package [27] to implement the RTI scheme described in Section VII. Since *acados* comes with a Python interface allowing rapid prototyping, we first tuned the algorithm in simulation and then used the generated C-code to perform real experiments. We employ the QP solver High-Performance Interior Point Method (HPIPM) [54], which exploits the sparsity structure of the MPC QP sub-problem (23), and supports inequality constraints.

The computation time required by the NMPC was in the range of 5-7 ms with the time horizon of 2 s and prediction horizon  $N$  equal to 50 on the on-board computer (a Quad Core Intel Pentium PC104 @ 1GHz) of HyQ for all the experiments. This computation time corresponds to the feedback phase of the RTI scheme where the QP (23) is solved after receiving the current state of the robot. The preparation phase of the RTI takes about 2-3 ms which is a fraction of the sampling time we chose. Refer to Section VII for more details on these phases of the RTI scheme.

3) *Integration with the locomotion framework*: The NMPC is integrated in a ROS node that publishes  $\mathbf{x}^p$  and  $\mathbf{u}^p$  at a frequency of 25 Hz. The on-board computer along with our locomotion framework (WBC Interface, WBC, etc., illustrated in Fig. 2) runs a node that subscribes to the topic of the NMPC ROS node. ROS is not a real-time operating system,

so it introduces quite a significant and unpredictable communication delay if the NMPC is run on an external (e.g. more powerful) computer. These delays are difficult to compensate for and they can cause the loss of synchronization between the NMPC ROS node and the WBC interface. Therefore, we decided to launch the NMPC node natively from the on-board computer to avoid the communication delays between two different computers. Even though we chose not to use a more powerful off-board computer for NMPC ROS node, we obtained a better performance in the overall implementation by avoiding the communication delays of ROS.

## B. Simulations

We show our NMPC planner in action on challenging terrain starting with simulations. These simulations are pallet crossing, walking over unstructured rough terrain and walk into a V-shaped Chimney.

1) *Pallet crossing*: In this simulation HyQ traverses pallets of different heights, placed at varying distances from each other. This simulation highlights the importance of including mobility in the NMPC formulation (2b). In particular, the simulation scenario includes a set of pallets, each one of 1 m length, with variable heights between 0.13 and 0.17 m and placed at unequal gap lengths ranging from 0.2 and 0.7 m. We performed multiple trials commanding the robot to move forward at different velocities i.e., 0.05 m/s and 0.1 m/s to show the repeatability of our approach. To avoid stepping on undesired locations such as pallet edges and to prevent foot or shin collisions, the nominal footholds were adjusted by using the VFA (see Section V-3). Figure 8 shows the results of five different trials for each of the commanded velocities. The middle plot shows the pitch angle  $\theta$  of the robot as it traverses the scenario. Since the robot is only commanded to move along its  $X$  direction with a constant forward velocity and the foot locations are provided as known quantities to the NMPC, the adjustment in pitch is the result of minimizing the deviation from the hip-to-foot position corresponding to high mobility for all four legs. Without this feature, the robot would maintain a constant horizontal orientation eventually reaching low mobility in some legs as shown in the attached video for a single pallet simulation.

We also showed in the accompanying video<sup>1</sup> the simulation of a walk on randomly generated rough terrain (using a tool by [55]) further stressing the advantages of mobility cost mentioned earlier.

2) *Walk into a V-shaped chimney*: In this simulation we show HyQ walking at 0.03 m/s commanded velocity in the  $X$  direction into a V-shaped chimney with friction coefficient  $\mu = 0.7$  and walls inclined at  $35^\circ$  to the ground. This simulation exploits the cone constraints and force robustness cost defined inside the NMPC formulation that is vital to achieve this walk successfully. The robot receives online an update of the map of the environment through an on-board camera to get the information about the normals at the location of the contact. These normals are used to formulate the force robustness cost

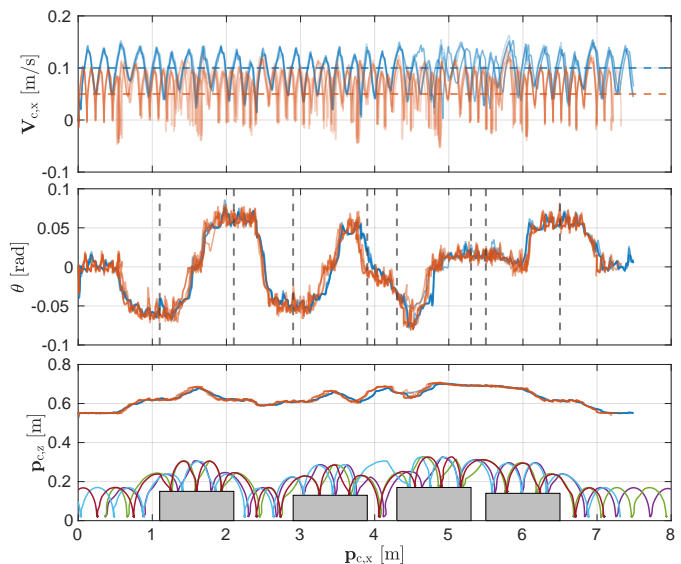


Fig. 8: Simulation of pallet crossing scenario for five different trials commanding the robot to cross at 0.1 m/s (blue) and 0.05 m/s (red). The top graph shows the actual velocities (solid lines) and their respective references (dashed lines). The graph in the middle shows the pitch angle and the dashed vertical lines indicate the edges of the pallets for that specific location in the plot. The bottom graph shows the CoM  $Z$  position for all the trials and the feet trajectories for one of the trials performed at 0.1 m/s. The color of swings are related to the different legs.

(2c) in the contact frame  $\mathcal{K}$ . With this cost, the NMPC provides optimal GRFs to stay close to the normals of friction cones at the contacts.

As shown in the accompanying video, without the cone constraints the robot slips while climbing the chimney and ultimately falls. When the force robustness cost is enabled, the forces are regularized to stay in the middle of the cones, thanks to the robustness feature described in Section IV-C. In this case the robot walks successfully into the chimney. In Fig. 9, it can be seen that the longitudinal and lateral components of the GRF at the Left-Front (LF) foot stay within the bound  $\mu f_z$  (in red) imposed by the cone constraints. Moreover, Fig. 10 plots the normal versus the resultant of  $X - Y$  components of the GRFs together with the cone bound  $\mu f_z$  (red line). The picture shows that the GRF stays well within the bound without any violation. Therefore, including the force regularization term enables the NMPC to account for the estimation error in the orientation of contact normals and increase robustness to the external disturbances.

Apart from the simulation mentioned above, we also have added in the attached video, the simulations regarding the kinematic robustness (see Section IV-B) and importance of the re-planning at a higher rate. For the kinematic robustness simulation, the robot is pushed with 200 N of lateral force for 1 s both in case of with (higher weight on GRFs  $Z$ ) and without (lower weight on GRFs  $Z$ ) ZMP margin. The ZMP margin plots for this simulation can be seen in Fig. 11 where the ZMP margin is improved in case of the red line compared to the blue one because the GRFs  $Z$  components are penalized relatively (100 times) more for the red line. Because of the

<sup>1</sup><https://www.dropbox.com/sh/mkr4pftcug6jlo7/AABNqu1AsGED2WSR8IqvaiUla?dl=0>

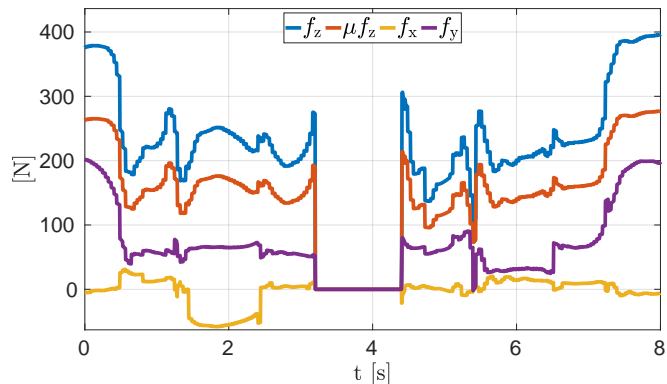


Fig. 9: Walk into a V-shaped chimney simulation: GRFs of LF leg for a single gait cycle with cone constraints and regularization cost. Both the longitudinal  $f_x$  and lateral  $f_y$  lie conservatively within the bound  $\mu f_z$  imposed by cone constraints.

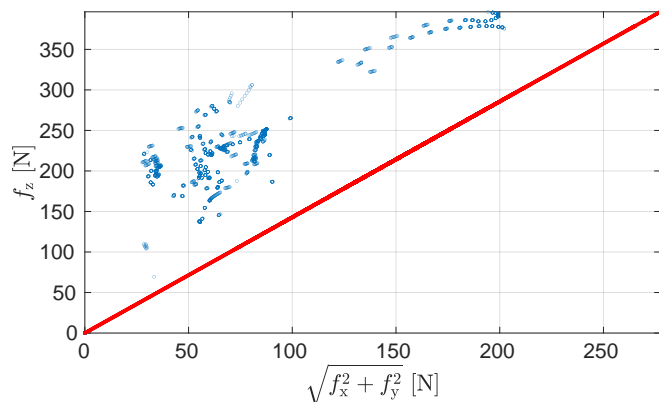


Fig. 10: Walk into a V-shaped chimney simulation: Normal force  $f_z$  versus resultant of X and Y forces  $\sqrt{f_x^2 + f_y^2}$  of the LF leg for a single gait cycle expressed in the contact frame. The red line is the cone bound  $\mu f_z$ .

improved margin the robot walks stably, whereas it falls while walking when there is no margin.

In second simulation, the robot is commanded with a constant CoM X velocity and heading velocity simultaneously. In case of re-planning at lower rate of 0.8 Hz, the robot becomes unstable and falls due to increase in the model uncertainties and tracking errors. We would like to stress that when the re-planning is done at a lower frequency than 25 Hz, the robot is in open-loop for the time interval between two consecutive re-planning instances, hence, it is not NMPC anymore but an online open-loop trajectory optimization. On the other hand, at a higher re-planning frequency of 25 Hz the robot walks successfully because the NMPC compensates for the model uncertainties and tracking errors.

### C. Experiments

We performed three different experiments to demonstrate the real-time implementation of our NMPC running on the on-board computer of the robot as follows.

1) *Omni-directional walk*: With this experiment, we wanted to show the omni-directional walk performed by HyQ with

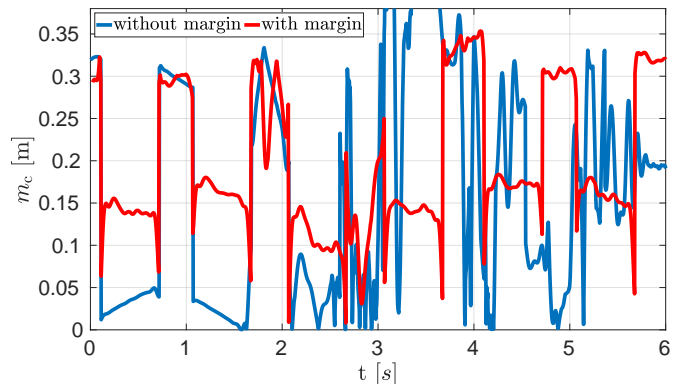


Fig. 11: Plot of the ZMP margin  $m_c$  used to measure locomotion stability. The robot is pushed immediately after 2s with lateral force of 200 N while walking on a flat terrain at 0.1 m/s CoM X velocity. The discontinuities are due to the switching between 3/4 stance legs in a crawl gait.

the NMPC on a flat terrain. This experiment validates that the NMPC computes feasible trajectories after receiving different velocity commands from the user while walking. In this experiment, the robot was commanded with a longitudinal velocity  $\mathcal{H}\mathbf{v}_{c,x}^{\text{usr}}$  by the user to walk forward/backward and then a lateral velocity. Finally, a heading velocity  $\omega_z^{\text{usr}}$  was commanded to turn in the left/right direction. Figure 12 shows the CoM X-Y position and yaw angle of the robot base and it can be noticed that the actual values follow very closely the planned trajectories provided by the NMPC. Figure 13 depicts the deviation of the actual velocities from the reference values while following the planned trajectories from NMPC. It can be seen in Fig. 14 that the GRFs generated by the WBC are compliant with the planned values  $\mathbf{u}^p$  and again the actual values of GRFs follow closely the planned values. From these plots, it can be observed that the continuous re-planning with NMPC plays an important role to achieve good tracking of the planned trajectory.

2) *Traversing a static pallet*: The purpose of this experiment was to demonstrate that the mobility cost (2b) incorporated in the NMPC formulation provides the necessary body pitch for the robot to traverse over a static pallet while maintaining good leg mobility. The pallet used in this experiment was 0.13 m in height and 0.8 m in length. Figure 15 shows that the robot pitches up while climbing up the pallet and pitches down consequently while climbing down from the pallet. As shown in the attached video in simulation, when the mobility cost is deactivated, the NMPC keeps the base orientation horizontal. This causes a reduced hip-to-foot distance while stepping up/down on the pallet ultimately resulting in low leg mobility. When mobility cost is activated, it directs the NMPC solution to achieve the necessary pitch that allows to maintain the hip-to-foot distance at the reference value and hence the leg mobility is improved. Moreover, the VFA provides the corrected foot position (i.e., to avoid shin or feet collisions with the edges of the pallet) to the NMPC and this further enhances the overall locomotion.

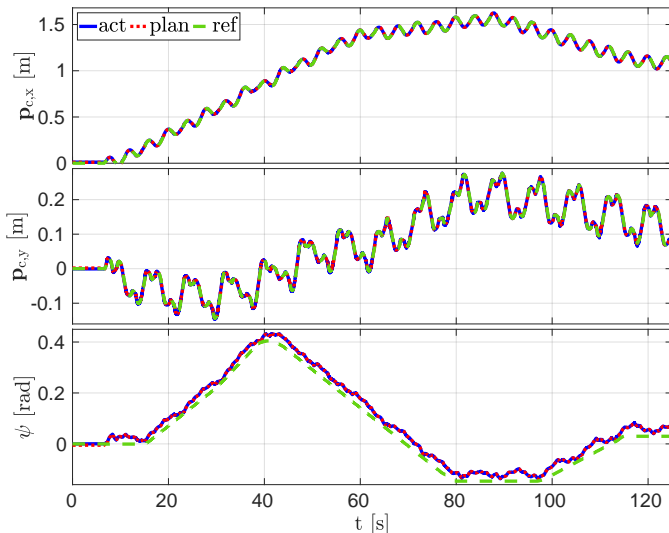


Fig. 12: CoM X-Y position and yaw  $\psi$  in omni-directional walk experiment. The blue, dotted red and dashed green line represent the actual, planned and reference values, respectively.

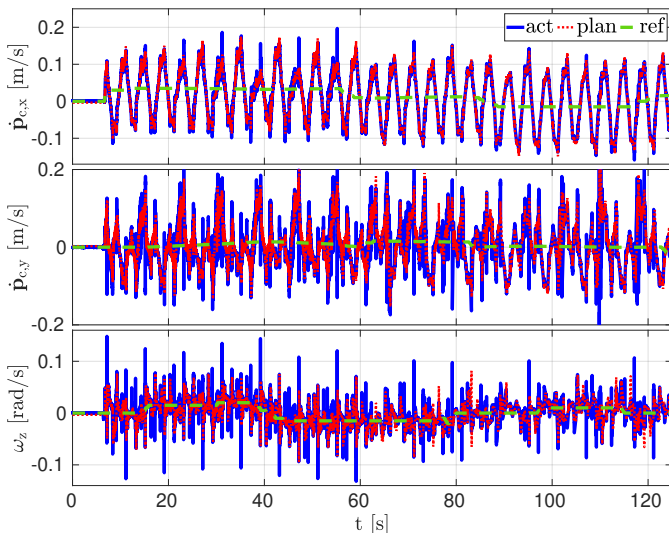


Fig. 13: The longitudinal  $\dot{p}_{c,x}$ , lateral  $\dot{p}_{c,y}$  and angular  $\omega_z$  velocity of the robot in omni-directional walk experiment. The blue, dotted red and the green line represent the actual, planned and reference values, respectively.

3) *Traversing a repositioned pallet* : In this experiment we tested our NMPC to plan the robot motion in real-time by adapting the changes in the environment with the help of VFA. As it can be seen from the attached video, when the pallet (0.13 m in height and 0.8 m in length) is pushed in front of HyQ while walking, the heightmap detects the pallet and the VFA provides updated foot locations to the NMPC. The NMPC after receiving these updated foot locations delivers a solution by pitching up the robot base in order to adapt to the change in the environment while maintaining the mobility. Even though the mobility cost is defined for the stance legs, it is interesting to notice that the NMPC decides to adjust the base pitch while swinging the RF leg onto the pallet (see Fig. 16) by forecasting the hip-to-foot distance at the

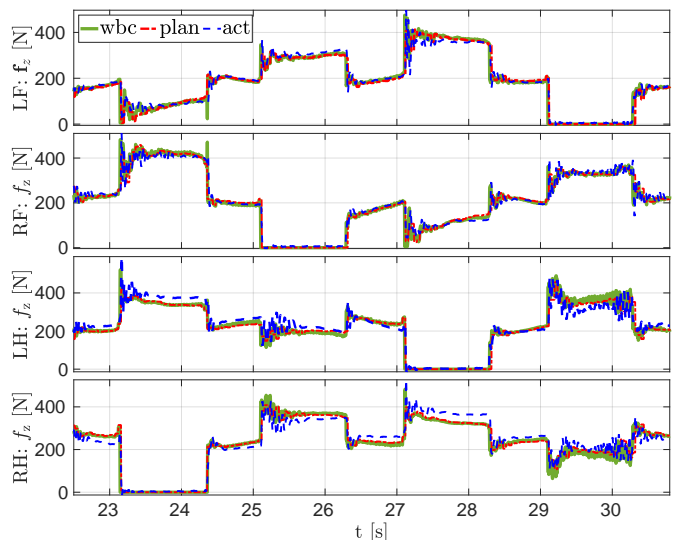


Fig. 14: GRFs of one gait cycle in the omni-directional walk experiment (We show only one cycle for better visibility of the data). The green, dotted red and dashed blue line represent the output from WBC i.e.,  $f_{z,i}^d$ , planned and reference values, respectively.

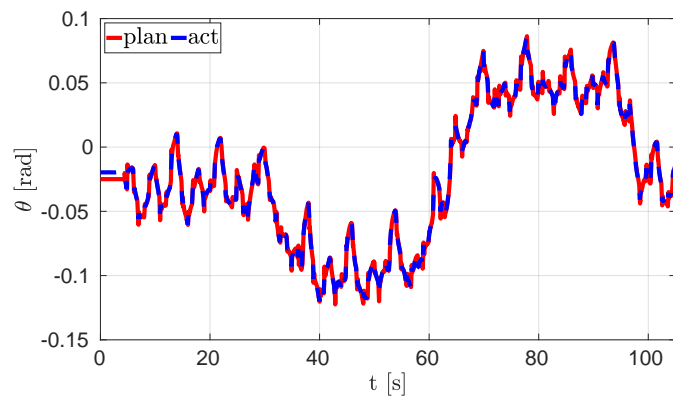


Fig. 15: Planned (red) and Actual (dashed blue) pitch of the robot base while traversing a static pallet in the experiment at a commanded CoM X velocity of 0.03 m/s.

touchdown. This experiment highlights the advantage of the predictive control over the traditional control approaches for its ability to incorporate the knowledge of the future states. It also validates the effectiveness of our mobility cost in the NMPC coupled with the VFA to adapt to the changes in the locomotion environment.

## IX. CONCLUSION

In this work we have developed a real-time NMPC that enhances the leg mobility of a quadruped robot for rough terrain locomotion with the help of a proposed mobility metric called mobility factor. The contact sequence parameters embedded inside the SRBD model allowed us to encode the complementarity constraints directly, and without a need to enforce these constraints separately in the NMPC. We exploited the RTI scheme for our NMPC that enabled us to close the loop at 25 Hz on the NMPC with a time horizon of 2 s. Closing the loop on NMPC at 25 Hz allowed us to compensate for the

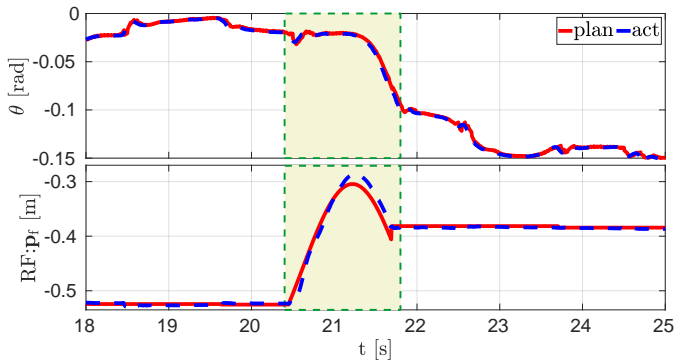


Fig. 16: Robot base pitch achieved during the swing of RF leg while traversing a repositioned pallet in the experiment a commanded CoM X velocity of 0.05 m/s. The red and dashed blue line are planned and actual values.

state drifts due to model uncertainties and tracking errors, and also adapt to the changes in the environment while following user commands both in the simulations and experiments.

In our NMPC, the mobility cost penalizes the hip-to-foot distance from a reference value corresponding to a high mobility factor and hence it directs the NMPC to compute essential robot orientation to maintain mobility while respecting the kinematic limits. This is evident from the pallet experiments where we also included the VFA to correct undesired foot positions defined by the heuristics and avoid possible shin collision. Including the kinematic robustness in our NMPC improved the locomotion stability of the robot in all of our experiments and simulation by keeping a sufficiently large ZMP margin from support polygon boundaries. Incorporating a force robustness term in the NMPC ensures that the GRFs stay close to the contact normals and hence, it enables the robot to cope with the estimation error of the orientation of the contact normals.

Our gait scheduler provides the contact sequences considering the user defined gait parameters and recovers the synchronization between planned and actual touchdown of the robot. This is essential when traversing rough terrain where premature or delayed touchdown could occur very frequently. The robocentric stepping strategy computes foot positions coherent with the base evolution avoiding error accumulation. The nominal foot positions supplied by the reference generator are further improved by the VFA that corrects the foot locations considering the terrain map.

With our NMPC we demonstrated successful dynamic locomotion in simulation as well as in the experiments on different rough terrains. In our future work we would like to extend our NMPC to optimize the step timing and foot locations. Additionally, the reference generator does not provide references by rejecting the external disturbances acting on the robot state, hence the robot complies transparently with these disturbances. Therefore, in the future we plan to empower the reference generator to reject disturbances to bring back the robot from a perturbed state to a state coherent with the user commands.

## APPENDIX ANGULAR VELOCITY

We employ the  $Z$ - $Y$ - $X$  convention [38] for the Euler angle vector  $\Phi = [\phi, \theta, \psi]^T$  to represent the orientation of the robot base where,  $\phi$ ,  $\theta$  and  $\psi$  are the roll, pitch and yaw, respectively. The angular velocity in inertial and CoM frame is related to the Euler angle rates with the following relations:

$$\omega = \mathbf{E}(\Phi) \dot{\Phi} \quad (25)$$

$${}^c\omega = \mathbf{E}'(\Phi) \dot{\Phi} \quad (26)$$

$\mathbf{E}(\Phi)$  and  $\mathbf{E}'(\Phi)$  are the *Euler angle rates matrix* and *conjugate Euler angle rates matrix* respectively given by,

$$\mathbf{E}(\Phi) = \begin{bmatrix} \cos(\theta) \cos(\psi) & -\sin(\psi) & 0 \\ \cos(\theta) \sin(\psi) & \cos(\psi) & 0 \\ -\sin(\theta) & 0 & 1 \end{bmatrix} \quad (27)$$

$$\mathbf{E}'(\Phi) = \begin{bmatrix} 1 & 0 & -\sin(\theta) \\ 0 & \cos(\phi) & \cos(\theta) \sin(\phi) \\ 0 & -\sin(\phi) & \cos(\theta) \cos(\phi) \end{bmatrix} \quad (28)$$

Remark:  $\mathbf{E}$  depends on pitch and yaw, whereas  $\mathbf{E}'$  on roll and pitch. Thus, the Euler angle rates  $\dot{\Phi}$  is

$$\dot{\Phi} = \mathbf{E}^{-1}(\Phi) \omega \quad (29)$$

$$\dot{\Phi} = \mathbf{E}'^{-1}(\Phi) {}^c\omega \quad (30)$$

## ACKNOWLEDGMENT

We would like to thank Jonathan Frey and Andrea Zanelli of IMTEK, University of Freiburg for their support with `acados` software. We also extend our gratitude to all the DLS lab members for their help in the experiments.

## REFERENCES

- [1] M. H. Raibert, *Legged robots that balance*. MIT press, 1986.
- [2] J. Pratt, C.-M. Chew, A. Torres, P. Dilworth, and G. Pratt, "Virtual model control: An intuitive approach for bipedal locomotion," *The International Journal of Robotics Research*, vol. 20, no. 2, pp. 129–143, 2001.
- [3] M. Focchi, R. Orsolino, M. Camurri, V. Barasuol, C. Mastalli, D. G. Caldwell, and C. Semini, *Heuristic Planning for Rough Terrain Locomotion in Presence of External Disturbances and Variable Perception Quality*. Springer International Publishing, 2020, pp. 165–209.
- [4] M. Focchi, A. del Prete, I. Havoutis, R. Featherstone, D. G. Caldwell, and C. Semini, "High-slope terrain locomotion for torque-controlled quadruped robots," *Auton. Robots*, pp. 1–14, 2016.
- [5] S. Fahmi, M. Focchi, A. Radulescu, G. Fink, V. Barasuol, and C. Semini, "STANCE: Locomotion adaptation over soft terrain," *IEEE Trans. Robot. (T-RO)*, vol. 36, no. 2, pp. 443–457, Apr. 2020.
- [6] C. D. Bellicoso, F. Jenelten, P. Fankhauser, C. Gehring, J. Hwangbo, and M. Hutter, "Dynamic locomotion and whole-body control for quadrupedal robots," in *2017 IEEE/RSJ International Conference on Intelligent Robots and Systems (IROS)*, 2017, pp. 3359–3365.
- [7] S. Kuindersma, F. Permenter, and R. Tedrake, "An efficiently solvable quadratic program for stabilizing dynamic locomotion," in *2014 IEEE International Conference on Robotics and Automation (ICRA)*, 2014, pp. 2589–2594.
- [8] M. Neunert, F. Farshidian, A. W. Winkler, and J. Buchli, "Trajectory Optimization Through Contacts and Automatic Gait

- Discovery for Quadrupeds,” *IEEE Robot. Autom. Lett.*, vol. 2, no. 3, pp. 1502–1509, 2017.
- [9] M. Posa, S. Kuindersma, and R. Tedrake, “Optimization and stabilization of trajectories for constrained dynamical systems,” in *2016 IEEE International Conference on Robotics and Automation (ICRA)*, 2016, pp. 1366–1373.
- [10] B. Aceituno-Cabezas, C. Mastalli, D. Hongkai, M. Focchi, A. Radulescu, D. G. Caldwell, J. Cappelletto, J. C. Grieco, G. Fernando-Lopez, and C. Semini, “Simultaneous Contact, Gait and Motion Planning for Robust Multi-Legged Locomotion via Mixed-Integer Convex Optimization,” in *IEEE Robot. Autom. Lett.*, 2018.
- [11] O. Melon, M. Geisert, D. Surovik, I. Havoutis, and M. Fallon, “Reliable trajectories for dynamic quadrupeds using analytical costs and learned initializations,” in *2020 IEEE International Conference on Robotics and Automation (ICRA)*, 2020, pp. 1410–1416.
- [12] M. Neunert, M. Stauble, M. Gifftthaler, C. D. Bellicoso, J. Carius, C. Gehring, M. Hutter, and J. Buchli, “Whole-Body Nonlinear Model Predictive Control Through Contacts for Quadrupeds,” *IEEE Robot. Autom. Lett.*, vol. 3, no. 3, pp. 1458–1465, 2018.
- [13] J. Koenemann, A. D. Prete, Y. Tassa, E. Todorov, O. Stasse, M. Bennewitz, and N. Mansard, “Whole-body model-predictive control applied to the HRP-2 humanoid,” in *IEEE/RSJ Int. Conf. Intell. Robot. Syst.*, 2015, pp. 3346–3351.
- [14] H. Dai, A. Valenzuela, and R. Tedrake, “Whole-body Motion Planning with Simple Dynamics and Full Kinematics,” *IEEE-RAS Int. Conf. Humanoid Robot.*, 2014.
- [15] D. E. Orin, A. Goswami, and S.-H. Lee, “Centroidal dynamics of a humanoid robot,” *Auton. Robots*, vol. 35, no. 2-3, pp. 161–176, jun 2013.
- [16] A. W. Winkler, C. D. Bellicoso, M. Hutter, and J. Buchli, “Gait and Trajectory Optimization for Legged Systems Through Phase-Based End-Effector Parameterization,” *IEEE Robot. Autom. Lett.*, vol. 3, no. 3, pp. 1560–1567, 2018.
- [17] G. Bledt, P. M. Wensing, and S. Kim, “Policy-regularized model predictive control to stabilize diverse quadrupedal gaits for the mit cheetah,” in *2017 IEEE/RSJ International Conference on Intelligent Robots and Systems (IROS)*, 2017, pp. 4102–4109.
- [18] J. Di Carlo, P. M. Wensing, B. Katz, G. Bledt, and S. Kim, “Dynamic locomotion in the mit cheetah 3 through convex model-predictive control,” in *2018 IEEE/RSJ International Conference on Intelligent Robots and Systems (IROS)*, 2018, pp. 1–9.
- [19] T. Horvat, K. Melo, and A. J. Ijspeert, “Model predictive control based framework for com control of a quadruped robot,” in *2017 IEEE/RSJ International Conference on Intelligent Robots and Systems (IROS)*, 2017, pp. 3372–3378.
- [20] A. Herdt, H. Diedam, P. B. Wieber, D. Dimitrov, K. Mombaur, and M. Diehl, “Online walking motion generation with automatic footstep placement,” *Advanced Robotics*, vol. 24, no. 5-6, pp. 719–737, 2010.
- [21] R. Grandia, F. Farshidian, R. Ranftl, and M. Hutter, “Feedback mpc for torque-controlled legged robots,” in *2019 IEEE/RSJ International Conference on Intelligent Robots and Systems (IROS)*, 2019, pp. 4730–4737.
- [22] J. Hauser and A. Saccon, “A barrier function method for the optimization of trajectory functionals with constraints,” in *Proceedings of the 45th IEEE Conference on Decision and Control*, 2006, pp. 864–869.
- [23] G. Lantoine and R. P. Russell, “A hybrid differential dynamic programming algorithm for constrained optimal control problems. part 1: Theory,” *Journal of Optimization Theory and Applications*, vol. 154, no. 2, pp. 382–417, Aug 2012.
- [24] H. Li and P. M. Wensing, “Hybrid systems differential dynamic programming for whole-body motion planning of legged robots,” *IEEE Robotics and Automation Letters*, vol. 5, no. 4, pp. 5448–5455, 2020.
- [25] H. Bock and K. Plitt, “A multiple shooting algorithm for direct solution of optimal control problems\*,” *IFAC Proceedings Volumes*, vol. 17, no. 2, pp. 1603–1608, 1984, 9th IFAC World Congress Budapest, Hungary, 2–6 July 1984.
- [26] M. Diehl, H. G. Bock, and J. P. Schlöder, “A real-time iteration scheme for nonlinear optimization in optimal feedback control,” *SIAM J. Control Optim.*, vol. 43, no. 5, pp. 1714–1736, 2005.
- [27] R. Verschuere, G. Frison, D. Kouzoupis, N. van Duijkeren, A. Zanelli, B. Novoselnik, J. Frey, T. Albin, R. Quirynen, and M. Diehl, “Acados - A modular open-source framework for fast embedded optimal control,” *arXiv*, 2019.
- [28] F. Farshidian, E. Jelavic, A. Satapathy, M. Gifftthaler, and J. Buchli, “Real-time motion planning of legged robots: A model predictive control approach,” in *Humanoid Robot. (Humanoids), 2017 IEEE-RAS 17th Int. Conf.* IEEE, 2017, pp. 577–584.
- [29] G. Bledt and S. Kim, “Implementing regularized predictive control for simultaneous real-time footstep and ground reaction force optimization,” in *2019 IEEE/RSJ International Conference on Intelligent Robots and Systems (IROS)*, 2019, pp. 6316–6323.
- [30] P. Fankhauser, M. Bjelonic, C. Dario Bellicoso, T. Miki, and M. Hutter, “Robust rough-terrain locomotion with a quadrupedal robot,” in *2018 IEEE International Conference on Robotics and Automation (ICRA)*, 2018, pp. 5761–5768.
- [31] O. Cebe, C. Tiseo, G. Xin, H.-c. Lin, J. Smith, and M. Mistry, “Online Dynamic Trajectory Optimization and Control for a Quadruped Robot,” *arXiv*, 2020.
- [32] C. Semini, N. G. Tsagarakis, E. Guglielmino, M. Focchi, F. Cannella, and D. G. Caldwell, “Design of hyq - a hydraulically and electrically actuated quadruped robot,” *IMEchE Part I: Journal of Systems and Control Engineering*, vol. 225, no. 6, pp. 831–849, 2011.
- [33] M. Diehl, H. G. Bock, H. Diedam, and P.-B. Wieber, “Fast Direct Multiple Shooting Algorithms for Optimal Robot Control,” in *Fast Motions in Biomechanics and Robotics*, Heidelberg, Germany, 2005.
- [34] S. Gros, M. Zanon, R. Quirynen, A. Bemporad, and M. Diehl, “From linear to nonlinear MPC: bridging the gap via the real-time iteration,” *Int. J. Control*, vol. 93, no. 1, pp. 62–80, 2020.
- [35] T. Boaventura, J. Buchli, C. Semini, and D. Caldwell, “Model-based hydraulic impedance control for dynamic robots,” *Robotics, IEEE Transactions on*, vol. 31, no. 6, pp. 1324–1336, Dec 2015.
- [36] S. Nobili, M. Camurri, V. Barasuol, M. Focchi, D. G. Caldwell, C. Semini, and M. Fallon, “Heterogeneous sensor fusion for accurate state estimation of dynamic legged robots,” in *Proceedings of Robotics: Science and Systems*, Boston, USA, July 2017.
- [37] P. Fankhauser and M. Hutter, “A Universal Grid Map Library: Implementation and Use Case for Rough Terrain Navigation,” in *Robot Operating System (ROS) – The Complete Reference (Volume 1)*, A. Koubaa, Ed. Springer, 2016, ch. 5.
- [38] J. Diebel, “Representing Attitude: Euler Angles, Unit Quaternions, and Rotation Vectors,” 2006.
- [39] R. Quirynen, “Numerical Simulation Methods for Embedded Optimization,” *Thesis*, no. January, p. 327, 2017.
- [40] J. C. Butcher, *Numerical Methods for Ordinary Differential Equations*. J. Wiley, 2003.
- [41] E. Hairer, S. Nørsett, and G. Wanner, *Solving Ordinary Differential Equations I*, 2nd ed., ser. Springer Series in Computational Mathematics. Berlin: Springer, 1993.
- [42] E. Hairer, S. Norsett, and G. Wanner, *Solving Ordinary Differential Equations II – Stiff and Differential-Algebraic Problems*, 2nd ed., ser. Springer Series in Computational Mathematics. Berlin: Springer, 1996.
- [43] O. Villarreal, V. Barasuol, P. M. Wensing, D. G. Caldwell, and C. Semini, “MPC-based controller with terrain insight for dynamic legged locomotion,” in *2020 IEEE International Conference on Robotics and Automation (ICRA)*, 2020, pp. 2436–2442.

- [44] A. B. Younes, J. D. Turner, D. Mortari, and J. L. Junkins, "A Survey of attitude error representations," 2012.
- [45] M. Focchi, R. Featherstone, R. Orsolino, D. G. Caldwell, and C. Semini, "Viscosity-based height reflex for workspace augmentation for quadrupedal locomotion on rough terrain," in *2017 IEEE/RSJ International Conference on Intelligent Robots and Systems (IROS)*, 2017, pp. 5353–5360.
- [46] L. Sciavicco, B. Siciliano, and B. Sciavicco, *Modelling and Control of Robot Manipulators*, 2nd ed. Berlin, Heidelberg: Springer-Verlag, 2000.
- [47] T. Yoshikawa, "Analysis and Control of Robot Manipulators with Redundancy," pp. 735–747, 1984.
- [48] C. Gehring, C. D. Bellicoso, S. Coros, M. Bloesch, P. Fankhauser, M. Hutter, and R. Siegwart, "Dynamic trotting on slopes for quadrupedal robots," in *2015 IEEE/RSJ International Conference on Intelligent Robots and Systems (IROS)*, 2015, pp. 5129–5135.
- [49] G. Raiola, E. Mingo Hoffman, M. Focchi, N. Tsagarakis, and C. Semini, "A simple yet effective whole-body locomotion framework for quadruped robots," *Frontiers in Robotics and AI*, vol. 7, p. 159, 2020.
- [50] P.-b. Wieber, "Trajectory free linear model predictive control for stable walking in the presence of strong perturbations," in *2006 6th IEEE-RAS International Conference on Humanoid Robots*, 2006, pp. 137–142.
- [51] T. Bretl and S. Lall, "Testing static equilibrium for legged robots," *IEEE Transactions on Robotics*, vol. 24, no. 4, pp. 794–807, 2008.
- [52] O. Villarreal, V. Barasuol, M. Camurri, L. Franceschi, M. Focchi, M. Pontil, D. G. Caldwell, and C. Semini, "Fast and continuous foothold adaptation for dynamic locomotion through cnns," *IEEE Robotics and Automation Letters*, vol. 4, no. 2, pp. 2140–2147, 2019.
- [53] R. Quirynen, M. Vukob, M. Zanon, and M. Diehl, "Autogenerating Microsecond Solvers for Nonlinear MPC: a Tutorial Using ACADO Integrators," *Optimal Control Applications and Methods*, vol. 36, pp. 685–704, 2014.
- [54] G. Frison and M. Diehl, "HPIPM: a high-performance quadratic programming framework for model predictive control," *arXiv*, 2020.
- [55] B. Abbyasov, R. Lavrenov, A. Zakiev, K. Yakovlev, M. Svinin, and E. Magid, "Automatic tool for gazebo world construction: from a grayscale image to a 3d solid model," in *2020 IEEE International Conference on Robotics and Automation (ICRA)*, 2020, pp. 7226–7232.